Dynamics and structural communication in the ternary complex of fully phosphorylated V2 vasopressin receptor, vasopressin, and β-arrestin 1

Luca Bellucci[a,b,1], Angelo Felline[a,1], Francesca Fanelli[a,c,*]

[a] Department of Life Sciences, University of Modena and Reggio Emilia, via Campi 103, 41125 Modena, Italy
[b] NEST, Istituto Nanoscienze-CNR, Piazza San Silvestro 12, 56127 Pisa, Italy
[c] Center for Neuroscience and Neurotechnology, University of Modena and Reggio Emilia, via Campi 287, 41125 Modena, Italy

ABSTRACT

G protein-coupled receptors (GPCRs) are critically regulated by arrestins, which not only desensitize G-protein signaling but also initiate a G protein-independent wave of signaling.

The information from structure determination was herein exploited to build a structural model of the ternary complex, comprising fully phosphorylated V2 vasopressin receptor (V2R), the agonist arginine vasopressin (AVP), and β-arrestin 1 (β-arr1). Molecular simulations served to explore dynamics and structural communication in the ternary complex.

Flexibility and mechanical profiles reflect fold of V2R and β-arr1. Highly conserved amino acids tend to behave as hubs in the structure network and contribute the most to the mechanical rigidity of V2R seven-helix bundle and of β-arr1. Two structurally and dynamically distinct receptor-arrestin interfaces assist the twist of the N- and C-terminal domains (ND and CD, respectively) of β-arr1 with respect to each other, which is linked to arrestin activation. While motion of the ND is essentially assisted by the fully phosphorylated C-tail of V2R (V2RCt), that of CD is assisted by the second and third intracellular loops and the cytosolic extensions of helices 5 and 6. In the presence of the receptor, the β-arr1 inter-domain twist angle correlates with the modes describing the essential subspace of the ternary complex. β-arr1 motions are also influenced by the anchoring to the membrane of the C-edge-loops in the β-arr1-CD. Overall fluctuations reveal a coupling between motions of the agonist binding site and of β-arr1-ND, which are in allosteric communication between each other. Mechanical rigidity points, often acting as hubs in the structure network and distributed along the main axis of the receptor helix bundle, contribute to establish a preferential communication pathway between agonist ligand and the ND of arrestin. Such communication, mediated by highly conserved amino acids, involves also the first amino acid in the arrestin C-tail, which is highly dynamic and is involved in clathrin-mediated GPCR internalization.

1. Introduction

G-protein-coupled receptors (GPCRs) control numerous cellular responses through the combined interplay of heterotrimeric G proteins, GPCR kinases (GRKs), and arrestins [1]. G proteins mediate activation of second-messenger-generating enzymes and other effectors [2], GRKs phosphorylate activated receptors [1], and arrestins subsequently bind phosphorylated receptors and cause receptor desensitization [3]. Arrestins activated by interaction with phosphorylated receptors can also mediate G-protein-independent signaling by serving as adaptors to link receptors to numerous signaling pathways [4], e.g. by recruiting several kinases including ERK1/2 [5,6].

Despite their central role in regulation and signaling of GPCRs, the functioning mechanism of β-arrestins is still poorly known. High-resolution information in that respect came from structure determinations [7–18], which revealed major structural differences between inactive and active states and possible binding modes to GPCRs. Binding modes at the atomic resolution between arrestin and a full-length GPCR were first inferred for visual bovine arrestin (named also arrestin 1) in complex with almost full-length phosphorylated rod opsin [15,17,19]. For non-opsin GPCRs, the first information at the atomic detail concerned β-arrestin 1 (β-arr1, named also arrestin 2) in complex with the fully phosphorylated C-tail of the vasopressin receptor type 2 (V2RCt) [12]. Incidentally, V2RCt provide the GPCR with high-affinity binding to β-arrestins [20]. When the present investigation was under review, the cryo-electron microscopy (cryo-EM) structures of β-arr1 in complex

with the chimera between M2-muscarinic receptor (M2R) and V2RCt (M2R/V2RCt [21]) and with the neurotensin receptor 1 (NTSR1 [22]) were released, providing advances in our understanding of β-arrestins recognition by GPCRs.

In the present study, the available information from structure determination was exploited to predict a ternary complex involving almost full-length fully phosphorylated and palmitoylated vasopressin receptor type 2 (V2R), its peptide agonist vasopressin (arginine-vasopressin (AVP)), and β-arr1. Microsecond molecular dynamics (MD) simulations in explicit membrane/water served to explore dynamics and allosteric communication in the ternary complex. The analysis of structural communication relied on the Protein Structure Network (PSN) analysis, a graph theory-based method, we implemented in the Wordom software [23] and in a webserver [24]. Applications of PSN analysis to members of the GTPase [25–27], GPCR [28–31], Rho Guanine Exchange Factor (RhoGEF) [32,33], PDZ domain [34], and integrins [35] allowed us to unveil relevant determinants of protein structure/function such as stability points, effects of misfolding mutations, triggers of constitutive activation, and allosteric communication.

The results of the present investigation highlighted the correspondence between mechanical rigidity points, evolutionary conservation, and structural communication within the ternary complex. Major collective motions of β-arr1 in interaction with both V2R and membrane, and the existence of a long-distance coupling between agonist binding site in V2R and the β-arr1 were unveiled. All those structural/dynamics features of the ternary complex appeared to be dependent on the full phosphorylation of V2RCt.

2. Theory/calculation

2.1. Model building of the ternary complex

Like the homologous members of the GPCR superfamily, V2R is characterized by seven transmembrane helices (H) organized in an up-down bundle architecture, with three intracellular and three extracellular loops (IL1–3 and EL1–3, respectively), as well as an extracellular N-terminus and a cytosolic C-terminus [36]. No crystallographic structures are available so far for this receptor. Available structural information concerns only the NMR structure of IL3 ("NMR structure of the intracellular loop (i3) of the vasopressin V2 receptor (GPCR)" (PDB ID: 2JX4)). The initial structural model of V2R (lacking N-terminus and C-terminus) in an active state was achieved by comparative modeling (by the Modeller software [37]), using the crystal structure of an active state of the μ-opioid receptor ("Crystal structure of active mu-opioid receptor bound to the agonist BU72" (PDB ID: 5C1M) [38]) as a template, according to a protocol already described [36,39]. To model the insertions, the following portions 94–97, 202–205, and 261–270 were deleted in the template crystal structure, followed by addition of external α-helical restraints to the segments: 58–64 (C-terminus of H1), 169–180 (C-terminus of H4), 197–204 (N-terminus of H5), 231–246 (cytosolic extension of H5), 253–264 (cytosolic extension of H6), and 330–342 (C-terminus of H8) of the target sequence. In that respect, the cytosolic extensions of H5 and H6 were consistent with the NMR structure of V2R IL3 (PDB ID: 2JX4). Five-hundred models were built by randomizing all the Cartesian coordinates of standard residues in the initial model. The best model according to quality checks was subjected to the application of rotamer libraries to those side chains in non-allowed conformation. β-arr1 from the crystallographic complex with the phosphorylated C-terminal tail of V2R ("Structure of active beta-arrestin1 bound to a G protein-coupled receptor phosphopeptide" (PDB ID: 4JQI) [12]) was completed with the missing side chains and whole residues (i.e. the 309–311 portion of a loop) by means of the "loop_model" routine of Modeller. One hundred loop models were built, by finally selecting the one with no bad main chain conformations and the lowest violation of stereochemical restraints. In this way, a complex between the completed β-arr1 and

V2RCt phosphorylated (p) at pT347, pS350, pS357, pT359, pT360, pS362, pS363, and pS364 (β-arr1-V2RCt) was achieved. The complex between V2R and β-arr1-V2RCt was built by fitting V2R and β-arr1-V2RCt, respectively, on opsin and visual arrestin in a crystallographic complex ("Crystal structure of rhodopsin bound to arrestin by femtosecond X-ray laser" (PDB ID: 4ZWJ) [15] and "Crystal structure of rhodopsin bound to visual arrestin" (PDB ID: 5DGY) [19]). Then, β-arr1/V2RCt was moved with respect to the V2R to relieve steric conflicts and to allow bridging (by Modeller) between the last amino acid of H8 (C342) and the first amino acid of V2RCt (R346). Twenty-one moves were probed by performing loop modeling of the 341–347 junction. Loop modeling served also to add the missing two-amino acid segment (354–355) in the V2RCt. The best model of phosphorylated V2R in complex with β-arr1 was palmitoylated at C341 and C342, in the C-terminus of V2R H8. A ternary complex with the crystal structure of the peptide agonist AVP ("Crystal Structure of trypsin-vasopressin complex" (PDB ID: 1YF4)) was achieved by using indications from site directed mutagenesis as a guide [40,41].

2.2. MD simulation setup

The structural model of the ternary complex between V2R, AVP, and β-arr1 was used as an input of MD simulations.

The N-terminus of both β-arr1 and V2R were acetylated, whereas the C-termini of β-arr1, V2R, and AVP were amidated. Two disulphide bridges were allowed to form between C112 and C192 in V2R and C1 and C6 in the peptide AVP. Furthermore, the highly conserved D85(2.50) and D136(3.49) (the labeling in parenthesis refers to a positional numbering widely used for GPCRs [42]) in V2R were kept in their protonated (neutral) states, consistent with evidences on the corresponding amino acid residues in rhodopsin [43,44], whereas H75 in V2R was kept in its protonated charged cationic state as it acts as a counterion of D67 in β-arr1.

Simulations were performed by NAMD2.11 [45] and were conducted in the NPT (constant particle Number, Pressure, and Temperature) ensemble. Periodic boundary conditions (PBC) were used and the long-range electrostatic interactions were treated with the particle-mesh-Ewald (PME) method [46]. The cutoff for non-bonded interactions was set to 10 Å and the switching function was applied to smooth interactions between 9 and 10 Å. The bonds between hydrogens and heavy atoms were constrained using the SHAKE algorithm [47], allowing for an integration step of 2 fs. The r-RESPA multiple time step method [48] was employed, allowing to update long-range electrostatic interactions every 4 fs and all the other interactions every 2 fs. Temperature was set to 310 K and regulated via a Langevin thermostat, while pressure was set to 1 atm and regulated via an isotropic Langevin piston manostat (as implemented in NAMD). The CHARMM36 force field was used for protein, membrane, phosphoryl, and palmitoyl groups, and counterions, whereas the TIP3P [49] force field was used for water.

Phosphorylated and palmitoylated V2R in complex with both AVP and β-arr1 was placed in the center of a phosphatidylcholine (1-palmitoyl-2-oleoyl-sn-glycero-3-phosphocholine, POPC) membrane generated exploiting the VMD Membrane Builder plugin [50]. POPC membrane held an initial surface (*xy*-plane) of 138×138 Å^2. Lipids within 1 Å from the protein complex were removed and the complex was placed along the *z*-axis, so that the center of mass of the receptor coincided with the center of the membrane (Fig. 1). The POPC-embedded protein ternary complex was then solvated and neutralized with 59 Na$^+$ and 64 Cl$^-$, reaching a salt concentration of about 0.05 mol/L. The final system consisted of 266.311 atoms in a cubic box of $150 \times 150 \times 150$ Å^3, which ensures correct decoupling between the periodic replica; the maximum extension of the whole protein complex was not greater than $110 \times 110 \times 110$ Å^3.

Energy minimization was carried out, followed by 4-ns equilibration of the membrane around the protein, while keeping the protein heavy
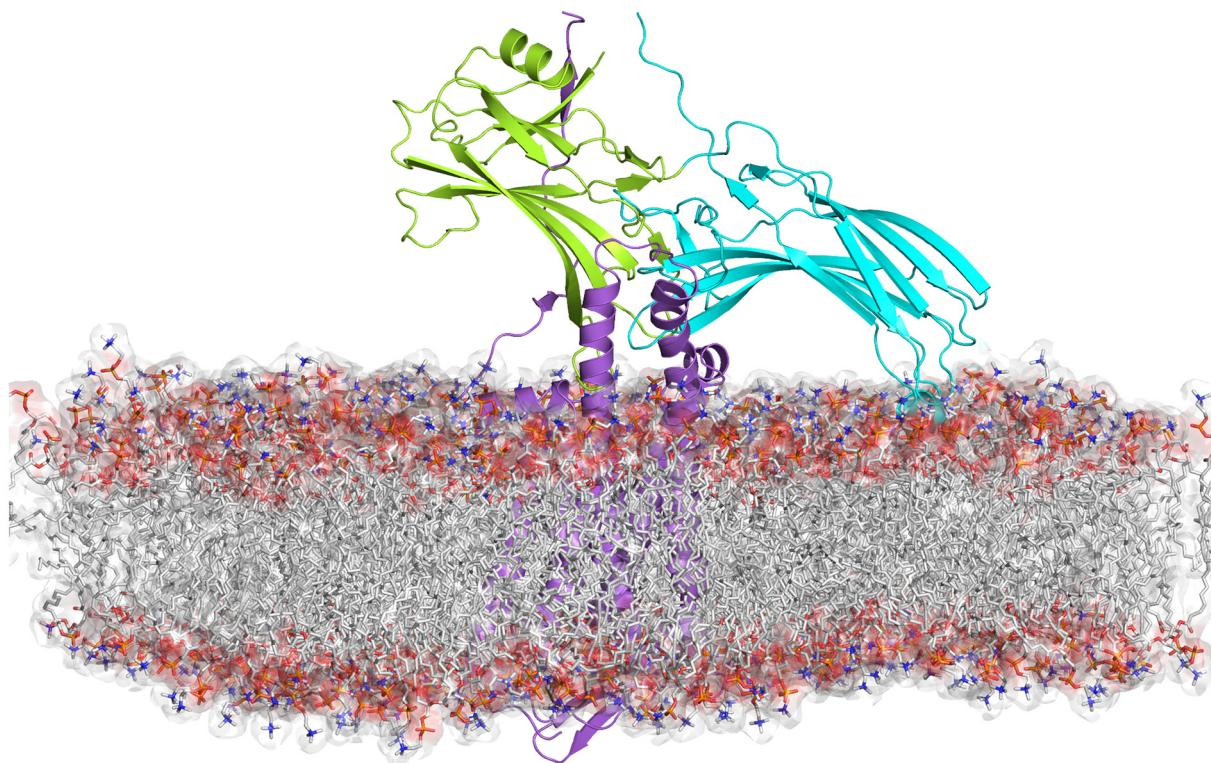
Fig. 1. Ternary complex embedded in the POPC membrane. The ternary complex involving V2R, AVP, and β-arr1 is shown, represented as cartoons, seen in a direction perpendicular to the helix-bundle main axis, the cytosolic side being on top. V2R is violet, AVP is black, the ND and CD of β-arr1 are, respectively, lemon-green and aquamarine. The heavy atoms of the POPC membrane are shown both in sticks and surface. The shown system is the first frame of the equilibrated MD trajectory. Palmitoyls, ions, and water are not shown. (For interpretation of the references to color in this figure legend, the reader is referred to the web version of this article.)

atoms harmonically constrained to their initial positions. The constraints over the protein were then removed and the system was further minimized. After minimization, the system was equilibrated for 100 ns. Box dimensions in the equilibrated system were about $138 \times 138 \times 137$ Å^3, being the z-axis free to move to keep the pressure constant. Such equilibration was followed by 1.5 μs production, by keeping the dimensions of the unit cell constant in the *xy*-plane, while allowing fluctuations along the *z*-axis.

During the production stage, distance restraints were applied to maintain selected inter-molecular contacts or secondary structures in V2R, according to experimental evidence [38,40,41]. In detail, α-helical restraints between the backbone oxygen atom at position i and the backbone nitrogen atom at position i + 4, excluding proline residues, were applied to: a) the segment 143–147 in IL2; and b) the segments 237–241 and 254–257 in cytosolic ends of H5 and H6. Furthermore, antiparallel β-sheet restraints were applied to the three H-bond-forming sites of the EL2 β-hairpin (i.e. positions 182, 184, and 186 in the N-terminal strand paired, respectively, with positions 193, 191, and 189 in the C-terminal strand). EL2, was, indeed, predicted to form a 2:2 β-hairpin with five amino acids per strand and a type-I′ turn (i.e. the SG sequence). Finally, distance restraints were also applied between selected atoms of V2R and AVP such as: a) respectively E40(CD)$_{V2R}$-P9(NT)$_{AVP}$, Q174(CD)$_{V2R}$-Q4(CD)$_{AVP}$, and Q291(CD)$_{V2R}$-N5(CG)$_{AVP}$.

2.3. MD analyses

2.3.1. Analyses of the intrinsic flexibility and of size/shape descriptors

Time series and distributions of the Cα-Root Mean Square Deviations (Cα-RMSDs), computed by means of the Wordom software [23] and concerning the equilibrated 1.5 μs trajectory are shown in Supplementary Fig. 1 (Fig. S1).

MD trajectories were subjected to a variety of analyses aimed at

inferring the intrinsic flexibility of the systems (i.e. Cα-Root Mean Square Fluctuations (Cα-RMSFs), force constants [51–53], overall fluctuations [54], and collective motions by Principal Component Analysis (PCA) [55]). All these analyses were performed by means of the Wordom software [23].

As for force constant analysis, the mechanical properties at the single residue level were inferred by computing the residue force constants through the analysis of the fluctuations of the mean distance d_i from each residue (to the rest of the structure) along the MD trajectory according to the following formula:

$$k_i = \frac{3k_B T}{\langle (d_i - \langle d_i \rangle)^2 \rangle} \tag{1}$$

where d_i is the mean distance defined above, $< >$ denotes the average over the simulation, k_B is the Boltzmann constant and T is the temperature of the simulation.

As for the overall fluctuation index Θ, whose computation was very recently implemented in Wordom, it is a measure of the intrinsic flexibility of the whole protein (or of a given sub-set of residues) and is proportional to the extent of conformational space explored in a simulation [54]. Θ is defined as root mean distance variance of each atom pair and is calculated by the following equation:

$$\Theta_{AB} = \sqrt{\frac{\sum_{i=1}^{N} \sum_{j=1}^{M} \frac{\sum_{k=1}^{F} (d_{ij}^k - \overline{d_{ij}})^2}{F}}{N \times M}} \tag{2}$$

where *A* and *B* are two sets of residues, *N* and *M* are the total number of atoms in set *A* and set *B*, respectively, and *F* is the total number of trajectory frames. Furthermore, d_{ij}^k is the distance between atom *i* from residue set A and atom *j* from residue set B in the *k*th frame while $\overline{d_{ij}}$ is the average distance between the same two atoms. Here, as residue sets we considered all Cα-atoms in: a) each helix and strand of both V2R and

β-arr1; b) the 225–273 portion of V2R comprising the cytosolic extensions of H5 and H6 and the interconnecting loop (IL3); c) the seven-helix bundle of V2R excluding the cytosolic extensions of H5 and H6 and IL3; d) EL2; e) the AVP peptide; f) AVP plus the binding site residues; g) each loop of β-arr1; and h) the N-terminal and C-terminal domains (ND: 6–172 amino acid segment and CD: 173–361 amino acid segment) of β-arr1.

Computations of all structural indices (e.g. distances, angles, and buried surface area) were carried out by Wordom as well. In that respect, the twist angle between ND and CD of β-arr1 was inferred by fitting either the crystal structures of active β-arr1 (PDB ID: 4JQI) or the trajectory frames with that of inactive β-arr1 ("Crystal structure of bovine beta-arrestin 1" (PDB ID: 1G4M) [9]). Indeed, herein the twist angle is the rotational angle needed to fit the backbone atoms of the two CD domains after fitting the backbone atoms of the two ND domains.

As for the analysis of the essential motions, PCA, the covariance matrices were built on the Cα-atoms of the MD trajectory. Similar to the computation of the Cα-RMSFs, PCA was carried out on all Cα-atoms of the ternary complex. Possible correlations between essential motions (PCs) and a number of descriptors were searched by the functional mode analysis (FMA) [56] implemented in Wordom. FMA is a method to identify a collective atomic motion related to a specific protein function. The method detects a collective motion (i.e. a mode) correlated with variations in a given quantity. A functional mode more often does not correspond to a specific normal mode or an essential mode but it results from a combination of a number of normal/essential modes. The twist angle between ND and CD of β-arr1 (see above) turned out to be linearly correlated (i.e. by Pearson correlation) with a combination of the first 100 eigenvectors (PCs). One-half trajectory was used to build the correlative model and the other half for model validation.

2.3.2. PSN analysis
2.3.2.1. Building of the protein structure graphs.
Building of the Protein Structure Graphs (PSG) was carried out by means of the PSN module implemented in the Wordom software [23]. PSN analysis is a product of graph theory applied to protein structures [57]. A graph is defined by a set of vertices (nodes) and connections (edges) between them. In a PSG, each amino acid residue is represented as a node and these nodes are connected by edges based on the strength of non-covalent interactions between residues [58]. The strength of interaction between residues i and j (I_{ij}) is evaluated as a percentage given by Eq. (3):

$$I_{ij} = \frac{n_{ij}}{\sqrt{N_i N_j}} \times 100 \tag{3}$$

where I_{ij} is the percentage interaction between residues i and j; n_{ij} is the number of atom-atom pairs between the side chains of residues i and j within a distance cutoff (4.5 Å); N_i and N_j are normalization factors for residue types i and j, which account for the differences in size of the amino acid side chains and their propensity to make the maximum number of contacts with other amino acids in protein structures.

Thus, I_{ij} are calculated for all node pairs. At a given interaction strength cutoff, I_{min}, any residue pair ij for which $I_{ij} \geq I_{min}$ is considered to be interacting and hence is connected. Node interconnectivity is used to highlight node clusters, where a cluster is a set of connected nodes in a graph. Cluster size, i.e., the number of nodes constituting a cluster, varies as a function of the I_{min}, and the size of the largest cluster is used to calculate the I_{critic} value. The latter is defined as the I_{min}, at which the size of the largest cluster is half the size of the largest cluster at $I_{min} = 0.0\%$. Studies by Vishveshwara's group found that optimal I_{min} corresponds to the one at which the largest cluster undergoes a transition [59].

The normalization factors for the 20 amino acids were derived from the work by Kannan and Vishveshwara [60], whereas the values for pSer, pThr, and palmitoyl were calculated for each trajectory frame, resulting in average normalization factors of 106.31, 123.75, and 83.4,

respectively. Glycines, excluded from the PSN analysis in previous applications [61], were included in this study.

Residues making zero edges are termed as orphans and those that make four or more edges are referred to as hubs at that particular I_{min}. Such cutoff for hub definition relates to the intrinsic limit in the possible number of non-covalent connections made by an amino acid in protein structures due to steric constraints. The cutoff 4 is close to the upper limit. The majority of amino acid hubs indeed make from 4 to 6 links, with 4 being the most frequent value.

Only those links and hubs present in at least 33% of the trajectory frames were defined as stable and considered for further analysis.

Finally, stable links were then used to highlight network communities, which are sets of highly interconnected nodes such that nodes belonging to the same community are densely linked to each other and poorly connected to nodes outside the community. Communities can be considered as fairly independent compartments of a graph. They were built by identifying all the k = 3-cliques, i.e. sets of 3 fully interconnected nodes, and then merging all those cliques sharing at least one node.

2.3.2.2. Search for the shortest communication paths.
The procedure has been previously described and validated [34]. Briefly, the search for all shortest paths relies on Dijkstra's algorithm [62]. The method first finds all possible communication paths between all node pairs, and then it filters the results according to the cross-correlation of atomic motions by the Linear Mutual Information (LMI) analysis [63]. Filtering consists in retaining only those shortest paths that contain one or more residues with a correlation ≥ 0.8 with at least one of the two path extremities (i.e. the first and last amino acids in the path). Filtered paths were used to build the global metapath, which is made of the most recurrent links, i.e. those links present in at least 20% of filtered paths. Such metapath represents a coarse/global picture of the structural communication in the considered system.

The relevance of each PSG link in a given global metapath was investigated by iteratively removing each link from the network and then recalculating the resulting global metapath. The effect of link removal on the formation of the native global metapath was then expressed as a fraction of native metapath links missing in the perturbed metapath.

2.4. Analysis of amino acid conservation

Conservation analysis was performed by using the ConSurf web server (http://consurf.tau.ac.il) [64]. In a typical ConSurf application, the query protein is first BLASTed against the UNIREF-90 database. Redundant homologous sequences are then removed using the CD-HIT clustering method. The resulting sequences are next aligned and the generated multiple sequence alignment (MSA) is used to reconstruct a phylogenetic tree. Given the tree and the MSA, the Rate4Site algorithm is used to calculate position-specific evolutionary rates under an empirical Bayesian methodology. The rates are normalized and grouped into nine conservation grades 1-through-9, where 1 includes the most rapidly evolving positions, 5 includes positions of intermediate rates, and 9 includes the most evolutionarily conserved positions [64].

We employed the human sequence of V2R and the sequence from the 4JQI crystal structure of β-arr1 (i.e. *Rattus norvegicus* sequence) as queries. Default conditions were used, but changing the minimal and maximal identity percentages to 20% and 80%, respectively, only for the V2R.

3. Results

3.1. Main structural features of V2R, β-arr1, and their complex

As a GPCR, the V2R holds an up-down bundle architecture and a rhodopsin 7-helix transmembrane-protein topology (Fig. 2A–C).

The V2R model employed in this study represents an agonist-bound
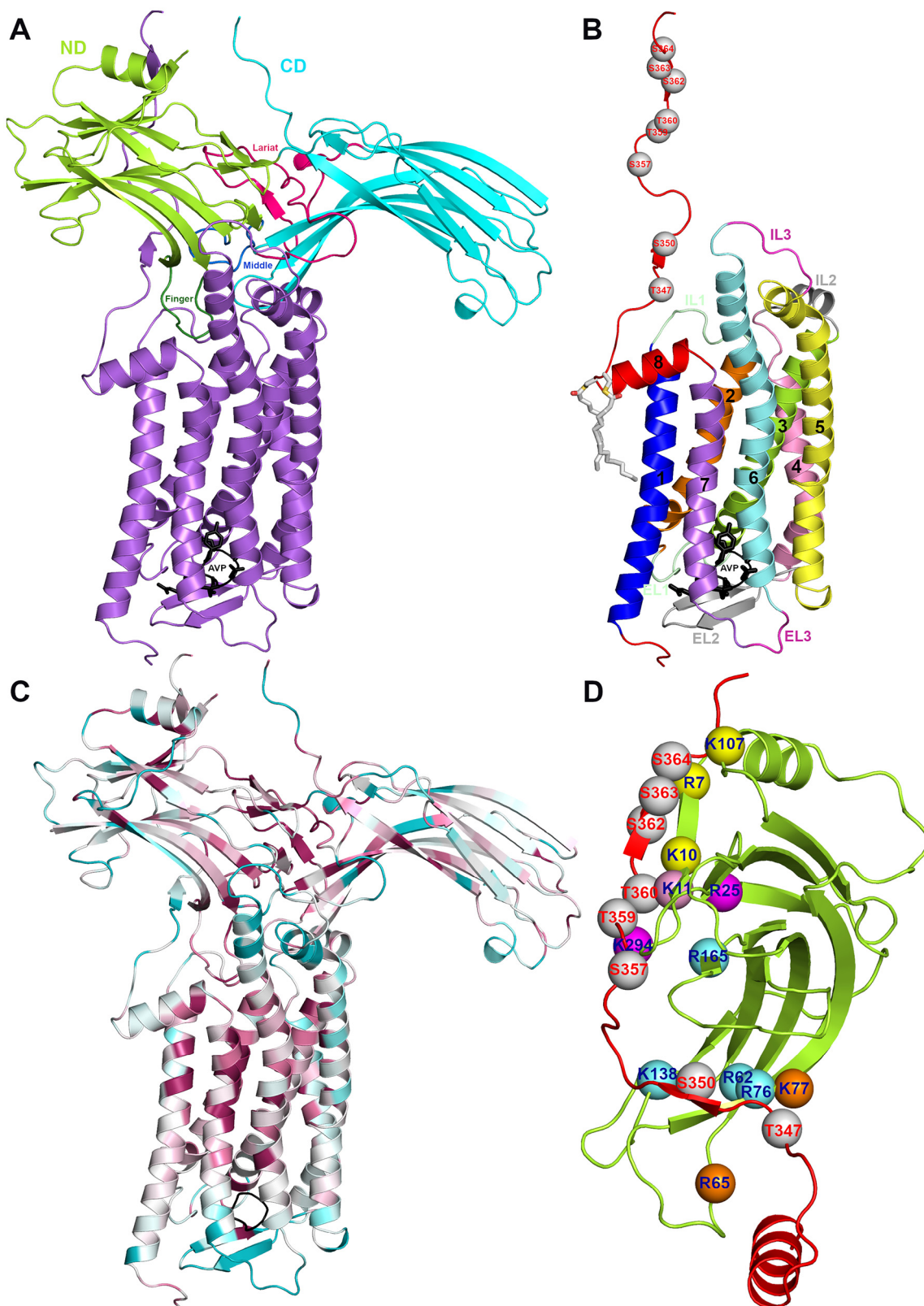
(caption on next page)

active state phosphorylated at pT347, pS350, pS357, pT359, pT360, pS362, pS363, and pS364 in the C-terminal tail (V2RCt) (Fig. 2C, D). Such active state is characterized by the absence of the salt bridge interaction between the E/DRY highly conserved arginine, R137(3.50), and the adjacent aspartate and by the detachment of the cytosolic end

of H6 from that of H3 due to an outward movement of the former.

The agonist AVP is a cyclic peptide due to a disulphide bridge between C1 and C6. It docks on the EL2 β-hairpin and makes a number of inter-side chain interactions with amino acid residues in H1 (i.e. R8$_{AVP}$-E40$_{V2R}$), H2 (i.e. F3$_{AVP}$-F91$_{V2R}$), H3 (i.e. Y2$_{AVP}$-Q119$_{V2R}$), H4 (i.e.

Fig. 2. Details of the predicted ternary complex. A. The ternary complex involving V2R, AVP, and β-arr1 is shown, represented as cartoons, seen in a direction perpendicular to the helix-bundle main axis, the cytosolic side being on top. V2R is violet and AVP, whose side chains are in sticks, is black. As for β-arr1, the ND and CD are, respectively, lemon-green and aquamarine, whereas finger, middle, and lariat loops are, respectively, forest, blue, and hot-pink. B. Only the V2R extracted from the complex is shown here. H1, H2, H3, H4, H5, H6, H7, and H8 are, respectively, blue, orange, lemon-green, pink, yellow, aquamarine, violet, and red, whereas N-terminus/C-terminus, IL1/EL1, IL2/EL2, and IL3/EL3 are, respectively, red, slate, gray, and magenta. The phosphorylated residues are represented as gray spheres centered on the Cα-atom. The heavy atoms of the two palmitoyl molecules are shown as sticks colored by atom type. The AVP peptide is represented as both cartoons and sticks colored black. C. In this panel, cartoons are colored according to the conservation grade of each amino acid. Such conservation, inferred by the ConSurf web server (http://consurf.tau.ac.il) [64], is quantified by scores that are translated in a color scale that goes from 1 (variable, cyan color) to 9 (very conserved, ruby color). D. Details of the interface between V2RCt and β-arr1 are shown. Phosphorylated residues on V2RCt are shown as gray spheres, whereas the cationic sites on β-arr1: A, B, C, and D are, respectively, shown as aquamarine, magenta, yellow, and orange, spheres respectively. The pink sphere concerns K11 that belongs to both cationic sites A and B.

All pictures concern the MD trajectory frame closest to the average structure. (For interpretation of the references to color in this figure legend, the reader is referred to the web version of this article.)

$Q4_{AVP}$-$Q174_{V2R}$), H6 (i.e. $N5_{AVP}$-Q291 and $Y2_{AVP}$-$F287_{V2R}$), and H7 (i.e. $C1_{AVP}$-$F307_{V2R}$ and $Y2_{AVP}$-$L310_{V2R}$).

β-arr1 holds a β-sandwich architecture and an immunoglobulin-like topology made of one N-terminal and one C-terminal domain (ND and CD, respectively). It represents an active state bound to V2RCt [12]. The overall structure of activated β-arr1 exhibits a wide variety of pronounced structural changes compared to previously determined in-active-state structures [9] (Fig. S2). Most notably, the ND and CD of β-arr1 hold a twist relative to one another, with a 20° rotation around a central axis [13].

The positions of pS357, pT360, and pS363 in V2R structurally overlap with positions of pT336, pS338, and E341 of opsin (Figs. 2B, D and 3A–D [17]). The three anionic sites in the GPCR C-tail recognize three corresponding positively charged pockets in arrestins denoted as A (K11, and R165 in β-arr1), B (K11, R25, and K294 in β-arr1), and C (K10 and K107 in β-arr1). Collectively, in the V2R-β-arr1 complex, site A recognizes pS350 (which is also close to R62, R76, and K138) and pS357; site B recognizes pT359 and pT360; and site C, which includes also the non-conserved R7, recognizes pS362, pS363, and pS364 (Fig. 2D). An additional cationic site unique to the V2R-β-arr1, herein

defined as site D (R65 and K77), recognizes pT347 (Fig. 2D).

Thus, the V2RCt binds to the ND at a similar location as the β-arr1 C-tail in inactive structures and makes extensive contacts. The latter primarily consist in charge-charge interactions between V2RCt phosphates and β-arr1 arginine and lysine side chains. Like the β-arr1 C-tail, V2RCt binds β-arr1 by extending the ND β-sandwich architecture. Unlike the C-tail, however, V2RCt binds as an antiparallel β-strand. This binding mode may serve as a general mechanism, by which arrestins recognize the phosphorylated loops and C-terminal tails of receptors [12].

Comparison of the inactive (PDB ID: 1G4M [9]) and V2RCt-bound active (PDB ID: 4JQI [12]) crystallographic structures of β-arr1 shows that, in addition to the inter-domain rearrangement, the ND and central loops show large structural changes associated with β-arr1 activation (Fig. S2). Several loops have been implicated in various aspects of β-arrestin activation and receptor interaction [9,16]. These include the finger loop (residues 64–72), the middle loop (residues 130–140), both participating in a central crest, and the lariat loop (residues 275–315), which comprises gate loop (residues 289–298) and back loop (residues 311–315). Each of these loops exhibits activation-dependent
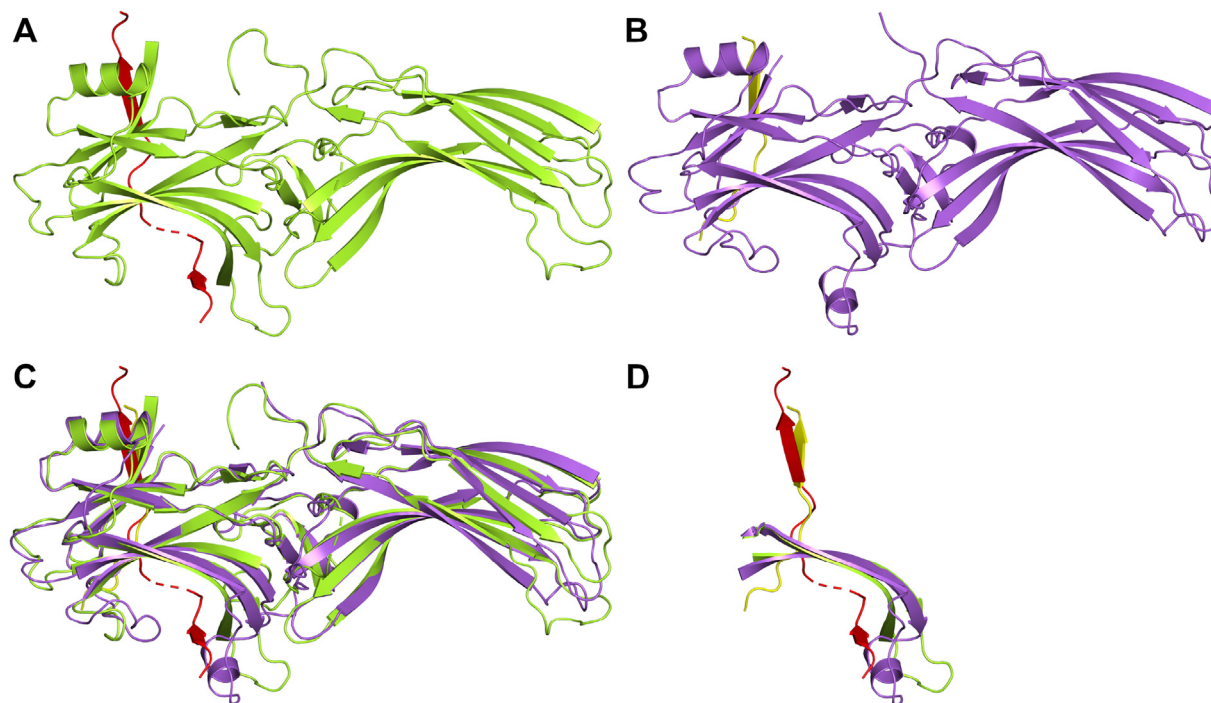
Fig. 3. Comparison between β-arr1 and visual arrestin. A. The cartoon representation of the crystal structure of β-arr1 (lemon-green) in complex with V2RCt (red) (PDB ID: 4JQI) is shown. B. The cartoon representation of the crystal structure of visual arrestin (violet) in complex with the C-tail of rod opsin (yellow) ("Crystal structure of rhodopsin bound to visual arrestin determined by X-ray free electron laser" (PDB ID: 5W0P)) is shown. C. The same structures as in A and B are shown superimposed at their Cα-atoms. D. Focus is put on the finger loop and the preceding and following strands as well as on the receptor C-tail from the two superimposed structures in C. (For interpretation of the references to color in this figure legend, the reader is referred to the web version of this article.)

conformational changes (Fig. S2). Comparison of these loops in the inactive and active structures of β-arr1 shows the considerable flexibility in each loop in the inactive conformation, but a more marked change in conformation upon β-arrestin activation.

The 4JQI crystal structure reveals that the V2RCt occludes the inactive conformation of the finger loop, which has been shown to be important for arrestin discrimination between active and inactive GPCRs [65]. V2RCt stabilizes an extended conformation of this loop by forming an anti-parallel β-sheet with the beginning of the strand that follows the loop, thus facilitating contact with the receptor core (Figs. 2 and 3). V2RCt interacts with the middle loop as well. Differently from the V2RCt, the phosphorylated C-tail of bovine opsin does not make any contact with the finger loop (which holds a two-turn helix) and the following strand, nor with the middle loop of visual arrestin (Fig. 3B–D) [17].

These elements likely lead to divergences in the way arrestins recognize V2R and opsin proteins. Remarkably, the finger loop holds a two-turn helix also in the crystal structure of β-arr2 (named also arrestin 3) bound to a non-receptor activator (hexakisphosphate (IP$_6$)) [18]. The divergent conformation of the loop in receptor-activated β-arr1 and IP6-activated β-arr2 ("active arrestin-3 with inositol hexakisphosphate" (PDB ID: 5TV1)) results in marked differences in the curvature of the preceding and following strands, the latter being unable to make an antiparallel β-sheet with V2RCt as seen for the structure of β-arr1 (Fig. S3). This suggests that the active states of β-arr2 induced by the fully phosphorylated C-tail of a GPCR and by IP6 are divergent.

When the present study was under review, the cryo-EM structures of β-arr1 in complex with M2R ("GPCR-Beta arrestin structure in lipid bilayer" (PDB ID: 6U1N) [21]) and NTSR1 ("neurotensin receptor and arrestin2 complex" (PDB ID: 6UP7) [22]) were released. Remarkably, the M2R, which holds phosphorylation sites in IL3 (missing in the structure) and not in the C-tail, is a chimera with the phosphorylated V2RCt (M2R/V2RCt). Differently, the NTSR1 holds six phosphorylation sites in the C-tail and four in IL3, both regions being almost totally unresolved in the structure [22]. Interestingly, the orientation of β-arr1 in complex with M2R/V2RCt is similar to that of visual arrestin in complex with opsin (Fig. 4A, B), the finger loops docking in the same receptor sites in the two complexes, in spite of the marked differences in conformation. In general, the conformation of all loops, in particular those in the central crest, diverges in the two arrestins. Moreover, β-arr1 is tilted approximately 7° further towards the membrane than visual arrestin, due to the more extended interactions between the C-edge loops and the membrane (Fig. 4A, B). Remarkably, in the complex with NTSR1, β-arr1 is even more tilted towards the membrane and is rotated approximately by 85° in the membrane plane compared to β-arr1 in complex with M2R/V2RCt or visual arrestin in complex with opsin (Fig. 4A–E) [17,21,22]. The crystal structure of β-arr1 in complex with fully phosphorylated V2RCt, here used for building the ternary complex, diverges from the structure of β-arr1 in complex with M2R/V2RCt (Fig. 4F, G). Major divergences concern the conformation and orientation of the finger loop that, in the M2R/V2RCt chimera, is no longer engaged in interaction with the phosphorylated V2RCt, which is not resolved in its N-terminal half (Fig. 4F, G). These differences, which may be linked, at least in part, to the possibility that only six out of eight sites are phosphorylated in the C-tail of the M2R/V2RCt chimera, cause a shift of β-arr1 in the complexes with the V2R modeled here and with the M2R/V2RCt chimera (Fig. 4H).

Other conformational switches of β-arr1 activation would include the portions: 88–96 (switch I (swI)), 175–190 (swII), 307–316 (swIII), and the C-terminus (swIV), according to inferences on β-arr2 [18].

Two major sets of intramolecular interactions have been proposed to constrain arrestins in an inactive conformation: the three-element interaction and the polar-core interaction [12]. The three-element interaction consists of interactions between β-strand 1 (β1), α-helix 1, and the C-tail of arrestin [66]. The salt bridges between V2RCt and sites A-C of β-arr1, with prominence to K10 and K11, induce displacement of

β-arr1 C-tail, which contains a clathrin binding site that has been previously characterized to be important for GPCR internalization [67]. Hence, displacement of the C-tail upon phosphopeptide binding and β-arr1 activation is probably an important contributor to clathrin-mediated GPCR internalization. The second constraint that stabilizes the inactive conformation of arrestins is the polar core [68] consisting of five interacting charged residues: D26, R169, D290, D297, and R393. Binding of V2RCt disrupts the polar core by displacing the arrestin C-tail and consequently removing R393 from the polar core. Residues D290 and D297 also lose interactions within the polar core, and this is accompanied by a marked twisting of the lariat loop, which contains both D290 and D297. Therefore, it is possible that disruption of the polar core is driven by the excess negative charge in this region following displacement of the arrestin C-terminus residue R393 [13]. Notably, the side chain of K294, a residue within the lariat loop, flips towards the ND upon activation and engages pT360 of V2RCt. It is possible that K294 recognition of phosphates provides an additional driving force for lariat-loop rearrangement, and may therefore stabilize β-arr1 in an active conformation [12].

The complex between V2R and β-arr1 predicted herein is characterized by two inter-protein interfaces. The primary interface is maintained by the formation of an anti-parallel β-sheet between the V2RCt and β-arr1 ND (i.e. β351-349$_{V2R}$-β73-87$_{β-arr1}$ and β361-365$_{V2R}$-β6-12$_{β-arr1}$), together with salt bridges between the eight phosphorylated residues in V2RCt and cationic amino acids in β-arr1 ND. As for the secondary interface, a) the β-arr1 finger loop docks in between V2R IL1 and H8; b) the middle loop makes contacts with both IL1 and the C-term of the V2R IL2; c) the gate loop makes contacts with the V2R IL2; d) the β-arr1 229–258 β-hairpin, comprising the C-loop (residues 242–246), makes contacts with V2R IL2 and the cytosolic ends of both H5 and H6; and e) the back loop makes contacts with the V2R IL3. The formation of the second interface is likely dictated by the establishment of the first interface. In particular, the docking mode of the finger loop onto the receptor core is strongly influenced by the formation of an anti-parallel β-sheet between the β-strand following the loop and V2RCt (Figs. 2–4). Such constraint is absent in the complexes between phosphorylated opsin and visual arrestin [17] and between the M2R/V2RCt chimera and β-arr1 [21] (Figs. 3 and 4). Molecular simulations here show that full phosphorylation of V2RCt, which also implicates persistent interactions between pT347 of V2RCt and the singular cationic D site of β-arr1, constraints the finger loop to dock in between H8 and IL1 of V2R, being unable to interact with H6, as found in the complexes between opsin and visual arrestin [15,17] or between M2R/V2RCt chimera and β-arr1 [21] (Figs. 3 and 4). Furthermore, such inter-molecular constraints, forbid the finger loop from interacting with H5 as inferred from cysteine cross-linking experiments on the complex between chimeric β2-adrenergic receptor (β2-AR/V2RCt) and β-arr1 [13]. Incidentally, the orientation of the β-arr1 in complex with β2-AR/V2RCt inferred from that study [13] would greatly diverge also from the orientation of the same arrestin in complex with M2R/V2RCt [21].

As for the relations between the ternary complex and the POPC-membrane, anchor points to the membrane surface include the two palmitoyls at the C-term of V2R H8 and the C-edge loops in the β-arr1 CD, i.e. 189–196 and 330–342, in particular the latter, which corresponds to the 344-loop of bovine visual arrestin that would engage the membrane upon formation of the high affinity opsin-arrestin complex [69]. Remarkably, the interactions predicted here between the C-edge loops of β-arr1 and the POPC-membrane are fully consistent with the recent evidence that one loop (189–196) contacts the membrane whereas the other (330–342) buries itself in the lipid bilayer (Fig. 1) [21].

3.2. Dynamics of V2R-arrestin complex

The flexibility of the ternary complex made by V2R, AVP, and β-arr1 simulated in explicit membrane/water was essentially investigated
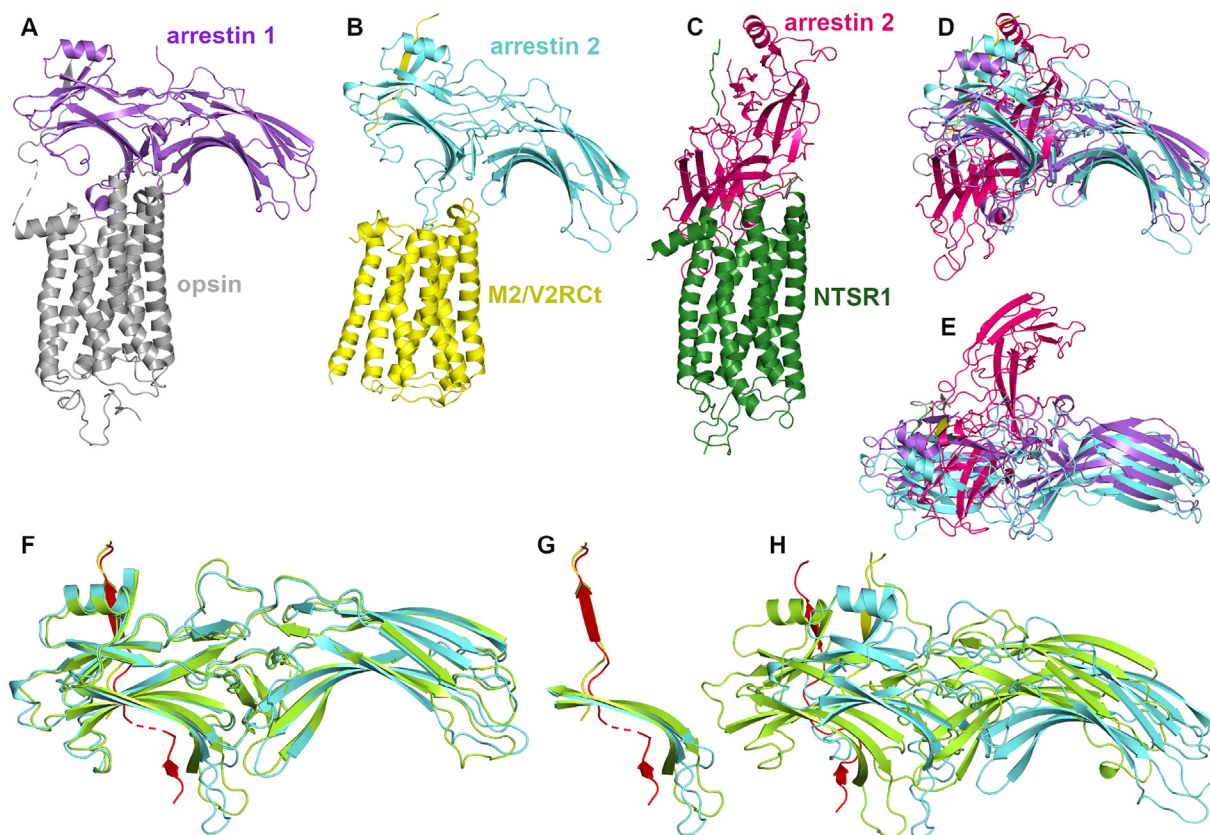
Fig. 4. Advances from structure determination of β-arr1-GPCR complexes. The complex between arrestin 1 (i.e. visual arrestin) and opsin (A) and the complexes between arrestin 2 (i.e. β-arr1) and M2R/V2RCt chimera (PDB ID: 6U1N) (B) and NTSR1 (PDB ID: 6UP7) (C) are shown as cartoons. Two views of the arrestin structures extracted from the three complexes (superimposed at the Cα-atoms of the receptor H3) are shown in panels D and E. In panel F, the structures 4JQI (β-arr1 is lemon-green, whereas V2RCt is red) and 6U1N (β-arr1 is aquamarine, whereas V2RCt is yellow) are shown superimposed at their Cα-atoms. G. Focus is put on the finger loop and the preceding and following strands as well as on the receptor C-tail from the two superimposed structures in F. H. The β-arr1 structures extracted from the complex with the V2R (i.e. the MD trajectory frame closest to the average; β-arr1 is lemon-green, whereas V2RCt is red) and from the cryo-EM complex with M2R/V2RCt (β-arr1 is aquamarine, whereas V2RCt is yellow) are shown, following superimposition of the Cα-atoms of the receptor H3. (For interpretation of the references to color in this figure legend, the reader is referred to the web version of this article.)

by the analyses of Cα-RMSDs, Cα-RMSFs, the time series of a number of stereochemical parameters, force constants [51–53], overall fluctuations [54], and collective motions [55].

The flexibility profiles, as accounted for by the Cα-RMSFs, of both V2R and β-arr1 reflect their topology in that peaks correspond to the loop regions and valleys to the secondary-structure elements (Figs. 5A and 6A).

The most flexible regions of V2R include the two termini, IL1, IL3, and EL3, whereas the most flexible regions of β-arr1 are the loops and, above all, the C-tail (truncated at P361), which no longer participates in the polar core as an effect of V2RCt binding. Complementary to the Cα-RMSF profiles, the peaks of mechanical rigidity, as accounted for by the force constants, correspond to the secondary structure elements (Figs. 5B and 6B). It is worth noting that big drop and increase in mechanical rigidity occur, respectively, in the cytosolic and extra-cellular halves of V2R H6, indicating that H6 has two dynamically distinct portions: the cytosolic half, more mobile, is deputed to arrestin binding, whereas the extracellular half, less mobile, is deputed to AVP binding (Fig. 5B). This dual behavior may have been emphasized by the interaction with β-arr1. Remarkably, for both receptor and arrestin, the highest force constant peaks (i.e. ≥ the average) correspond to highly conserved amino acids (i.e. holding ConSurf grades ≥ 7). The coupling between high amino acid conservation and force constant peaks is evident for almost all helices of V2R and the majority of β-strands of β-arr1 (Table S1 and Figs. 5B and 6B). As an example, the highest peaks in H1, H2, H6, and H7 of V2R correspond to some of the most conserved

amino acids in the helix (e.g. N55(1.50), D85(2.50), W284(6.48), and N321(7.49)). Noteworthy, the average force constant of V2R amino acids is lower (12.92 kcal mol^{-1} Å^{-2}) than that of β-arr1 (20.54 kcal mol^{-1} Å^{-2}), likely related to differences in fold between the two proteins. Collectively, the majority of amino acid residues with force constants well above average (i.e. with values ≥ twice the average) are highly conserved amino acids, i.e. 72% for V2R and 54% for β-arr1 (Table S1).

The overall fluctuation is a measure of the intrinsic flexibility of the whole protein (or of a given sub-set of residues) and is proportional to the extent of conformational space explored in a simulation (see the Theory/Calculation section). The overall fluctuation index is defined as a root mean distance variance, along the MD trajectory, of each atom in pairs of residue sets. In the present study, as residue sets we considered all Cα-atoms in each α-helix, β-strand, or loop, as well as in the whole ND and CD of β-arr1, and in the AVP agonist. The largest overall fluctuations, shown in Fig. 7A, B, turned out to be inter-molecular as they concerned the single strands or loops of β-arr1 vs a) EL2 of V2R (Fig. 7A) or b) AVP plus the AVP binding site residues (AVP-BS) (Fig. 7B, C). These data show that there is a coupling in terms of distance variance between AVP and β-arr1 portions. Remarkably, ND of β-arr1 and the single strands or loops in that domain contribute to the overall fluctuations with the AVP-BS more than CD or the single strands or loops in that domain (Fig. 7A, B).

Remarkably, in line with the overall fluctuations, high percentages of residues in the ND and AVP plus AVP-BS display correlated motions (Fig. S4). High percentages of correlated residues also concern ND and
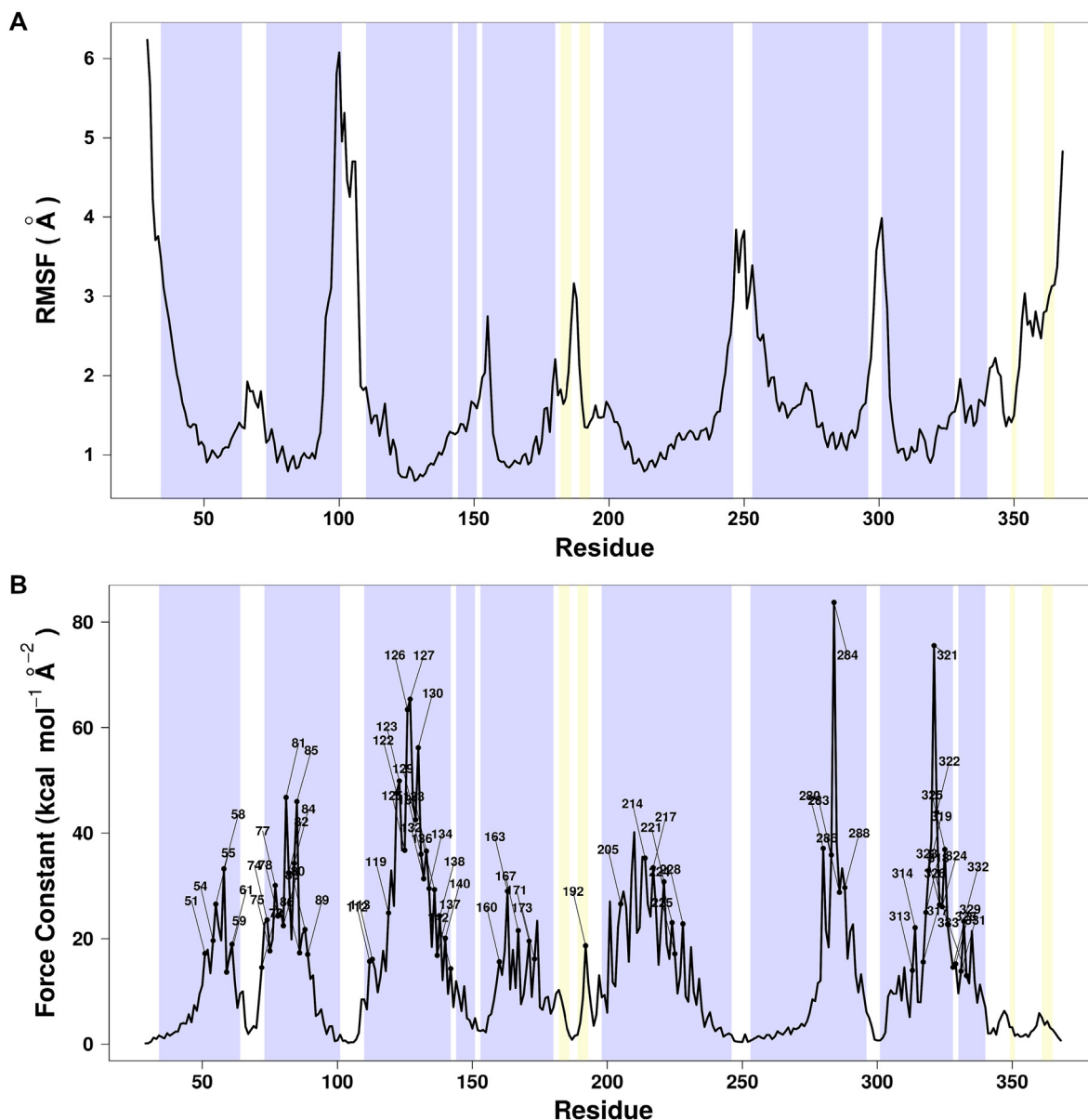
Fig. 5. Flexibility and mechanical profiles of V2R. The Cα-RMSFs (A) and mechanical (B) profiles of V2R in complex with β-arr1 are shown. Background colors indicate the secondary structure of the amino acid residues, where violet, yellow, and white indicate, respectively, α-helices, β-strands, and loops. The numbers on mechanical profiles highlight the amino acids holding both force constant ≥ the average and ConSurf conservation color ≥ 7. (For interpretation of the references to color in this figure legend, the reader is referred to the web version of this article.)

V2RCt, whereas pairs of residues in ND and CD do not display significantly correlated motions, suggesting lack of dynamic coupling in the latter case (Fig. S4).

The essential dynamics of the V2R-AVP-arrestin complex by fitting all Cα-atoms was described in great part by the first three eigenvectors or principal components (PCs), which account for 52% of total variance. In detail, the first principal component, PC1, is characterized by collective rotations about the complex main axis of β-arr1 domains and selected portions of V2R including the extracellular half of the helices, the three extracellular loops, the cytosolic extensions of H5 and H6 and their interconnecting loop (i.e. H5-I3-H6), and the C-tail that is integral with the β-arr1 ND (Fig. 8A). The AVP ligand contributes to PC1 as well. PC2 is characterized by collective rotations about the β-arr1 long axis of β-arr1, the extracellular regions and the C-tail of V2R, and AVP (Fig. 8B). Finally, PC3 concerns collective rotations about the β-arr1 short axis of β-arr1 and V2RCt (Fig. 8C).

A 21° twist angle between ND and CD of β-arr1 inferred by comparing the crystal structure of active β-arr1 (PDB ID: 4JQI) with that of inactive β-arr1 (PDB ID: 1G4M) was associated with formation of the activated state [12]. Monitoring such angle along the trajectory led to a median value of 13.1 ± 2.8°, indicating that the inter-domain twist does not experience marked fluctuations in the presence of the receptor, while tending to be slightly smaller compared to the active 4JQI structure (Fig. S5).

Functional mode analysis (FMA) found that the inter-domain twist angle is correlated with the collective atomic motions describing the essential subspace of the ternary complex (Fig. S6). The essential subspace (ES) is given by a variable number of eigenvectors whose associated eigenvalues account for 90% of the total variance of the Cα-displacements in a trajectory. In this case, the twist angle was found correlated ($R^2 = 0.93$) with a combination of the first 100 eigenvectors describing 96% of the total variance of the Cα-displacements (i.e. the ES) (Fig. S6A–D). In such combination, PCs were weighted based on their contribution to the FMA correlative model. The eigenvectors
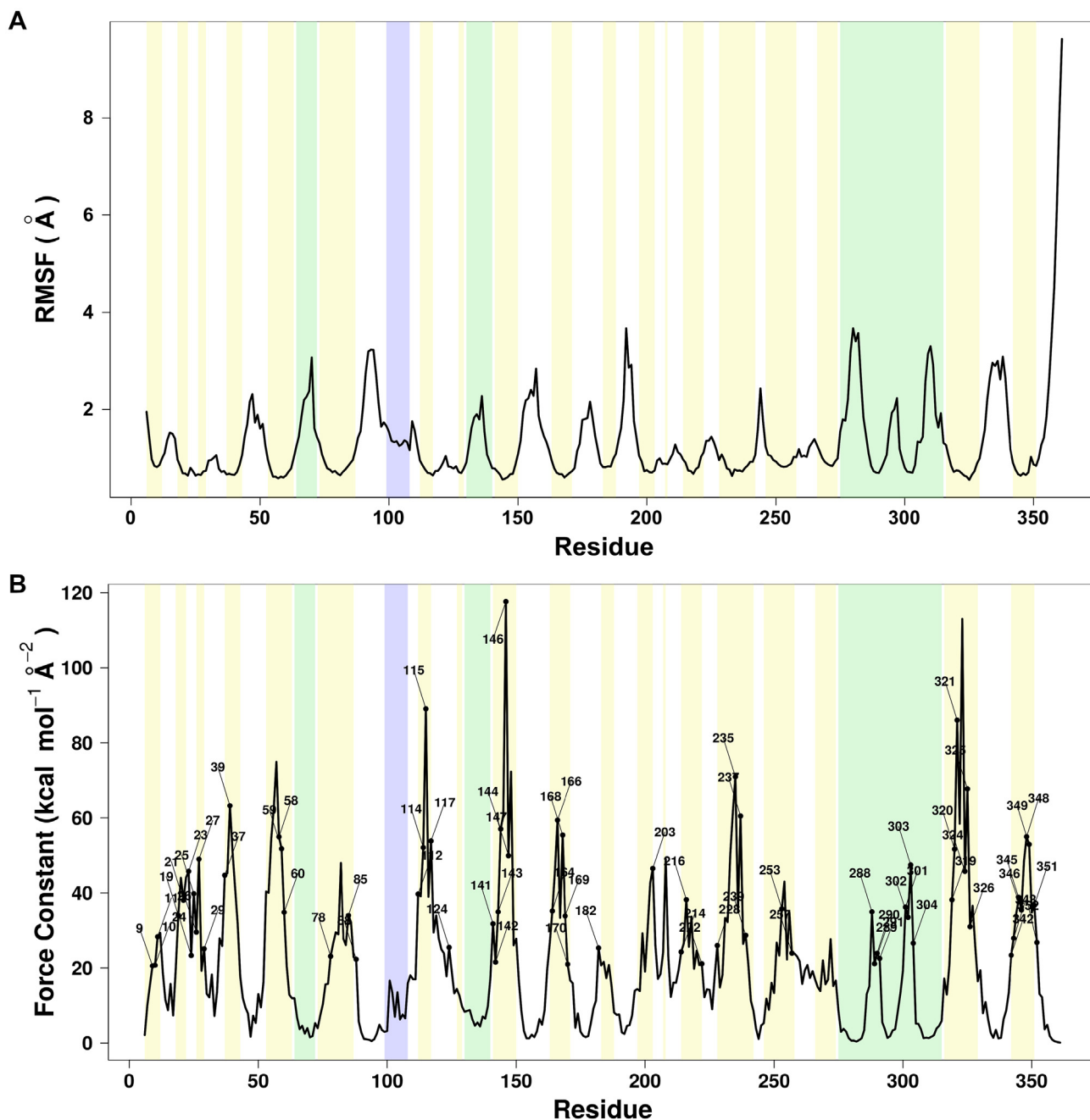
Fig. 6. Flexibility and mechanical profiles of β-arr1. The Cα-RMSFs (A) and mechanical (B) profiles of β-arr1 in complex with V2R are shown. Background colors indicate the secondary structure of the amino acid residues, where violet, yellow, and white indicate, respectively, α-helices, β-strands, and loops. Background green refers to finger, middle, and lariat loops. The numbers on mechanical profiles highlight the amino acids holding both force constant ≥ the average and ConSurf conservation color ≥ 7. (For interpretation of the references to color in this figure legend, the reader is referred to the web version of this article.)

contributing the most to the variance of the correlative model were PC1, PC12, and PC13 (Fig. S6E), accounting, respectively, for 27.5%, 1.34%, and 1.08% of the total variance of the Cα-displacements. The projections on the Cα-atoms of such combination of the first 100 eigenvectors provide hints on the contribution of the receptor. Indeed, inter-domain twist, linked to the two arrestin domains behaving as dynamically independent from each other, appeared assisted by the receptor. On one hand, the phosphorylated C-tail assists rotation of ND by interacting with the finger loop and the following strand, as well as with the cationic sites A-C; on the other, IL2, IL3, and the cytosolic extensions of H5 and H6 assist the rotation of CD by interacting with C-loop and the following strand as well as with gate and back loops.

β-arr1 motions are also influenced by the anchoring to the

membrane. In that respect, the C-edge loops in the β-arr1 CD, i.e. 189–196 and 330–342, in particular the latter, permanently make contacts with the membrane, essentially by van der Waals interactions between hydrophobic residues in the C-edge loops (e.g. mainly leucines) and the hydrophobic tails of phospholipids. Other interactions include salt bridges between aspartate residues in the C-edge loops and the cationic heads of POPC choline. All together, these interactions keep CD closer to the membrane surface than ND (Figs. 1 and S7). The distances between membrane plane and geometric center of either ND or CD hold, respectively, median values of 30.3 ± 1.9 Å and 20.6 ± 1.7 Å along the trajectory, thus reflecting a persistent tilt of β-arr1 towards the membrane (Figs. 1 and S7).

Collectively, the analysis of flexibility led to the following
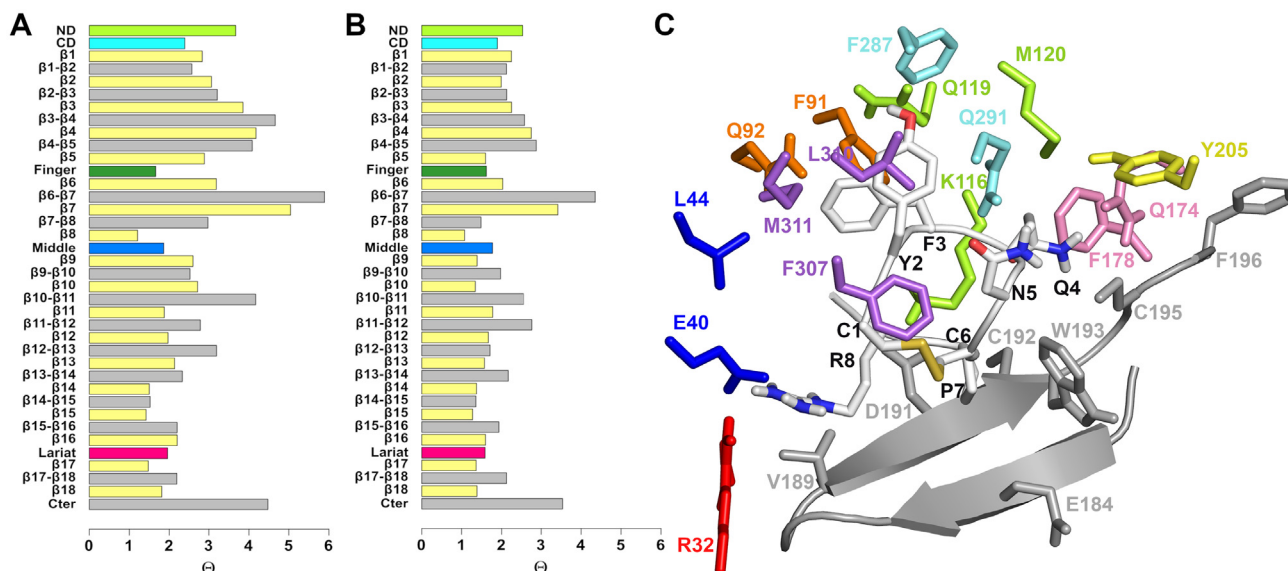
Fig. 7. Intermolecular overall fluctuations. (A) The overall fluctuations between distinct portions of β-arr1 and EL2 of V2R are plotted. (B) The overall fluctuations between distinct portions of β-arr1 and AVP plus AVP-BS are plotted. The AVP-BS amino acids included in calculations were those, in which at least one atom fell within a 5 Å-ray sphere from any atom of AVP in ≥90% of trajectory frames. Histograms are colored according to the β-arr1 portions, where β-strands, loops, finger loop, middle loop, lariat loop, and ND are, respectively, yellow, gray, dark-green, blue, hot-pink, and lemon-green, respectively. In panel C, EL2 and the side chains of AVP-BS amino acids (read their definition here above) are shown, respectively, as cartoons and sticks colored according to the V2R portion they belong to. In detail, H1, H2, H3, H4, H5, H6, H7, and H8 are, respectively, blue, orange, lemon-green, pink, yellow, aquamarine violet, and red, whereas N-terminus, EL1, EL2, and EL3 are, respectively, red, slate, gray, and magenta. (For interpretation of the references to color in this figure legend, the reader is referred to the web version of this article.)

highlights. 1. Flexibility and mechanical profiles reflect the folds of V2R and β-arr1, which is linked to function. 2. Highly conserved amino acids contribute the most to the mechanical rigidity of V2R seven-helix bundle and of β-arr1. 3. Overall fluctuations reveal a coupling between motions of the agonist plus its binding site and the ND of β-arr1. 4. β-arr1 is characterized by two dynamically distinct domains, ND, integral with V2RCt, and CD, anchored to the membrane surface. 5. In the presence of the GPCR, the β-arr1 inter-domain twist correlates with a combination of the modes describing the essential subspace visited by the ternary complex and is assisted by distinct interactions of V2R with each arrestin domain.

3.3. Structure network analysis

Structure network analyses relied on hub and community distributions, as well as on the computation of the shortest communication pathways (Figs. 9 and 10; Tables S2–S4).

Hubs and communities, respectively, highlight hyperlinked nodes and hyperlinked regions in a network. Indeed, whereas by definition hubs are nodes involved in at least four links, communities are sets of highly interconnected vertices such that nodes belonging to the same community are densely linked to each other and poorly connected to nodes outside the community. It is worth noting that hub computation here neglected both membrane and water. Mapping hubs and communities may indirectly provide the determinants of flexibility
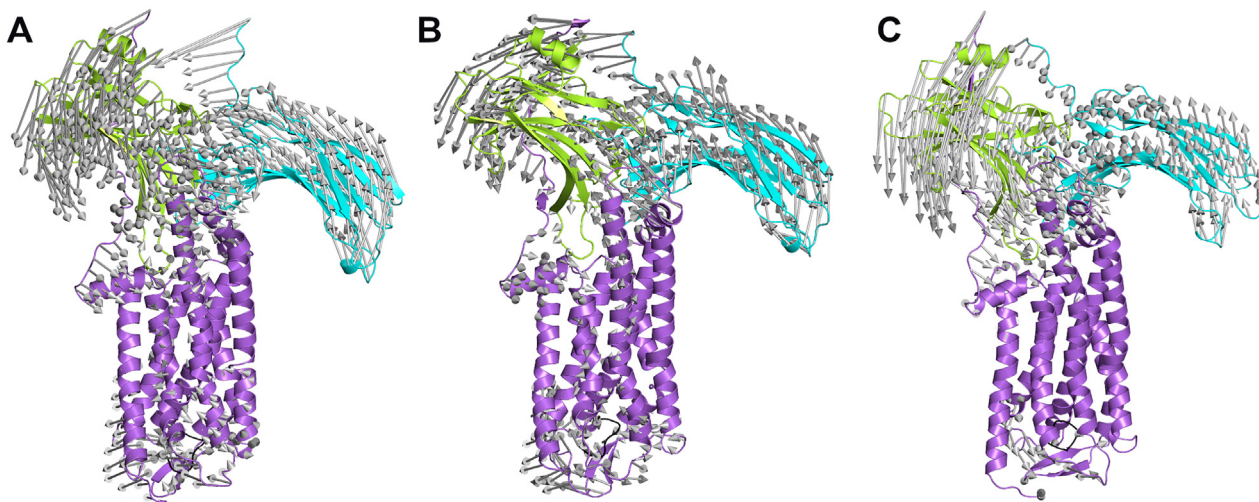
Fig. 8. Essential motions of V2R-arrestin complex. The porcupine representations of PC1 (left), PC2 (center), and PC3 (right) are shown on the cartoons of the ternary complex involving V2R, AVP, and β-arr1. The receptor is violet, the AVP ligand is black, whereas the ND and CD of β-arr1 are lemon-green and aquamarine, respectively. (For interpretation of the references to color in this figure legend, the reader is referred to the web version of this article.)
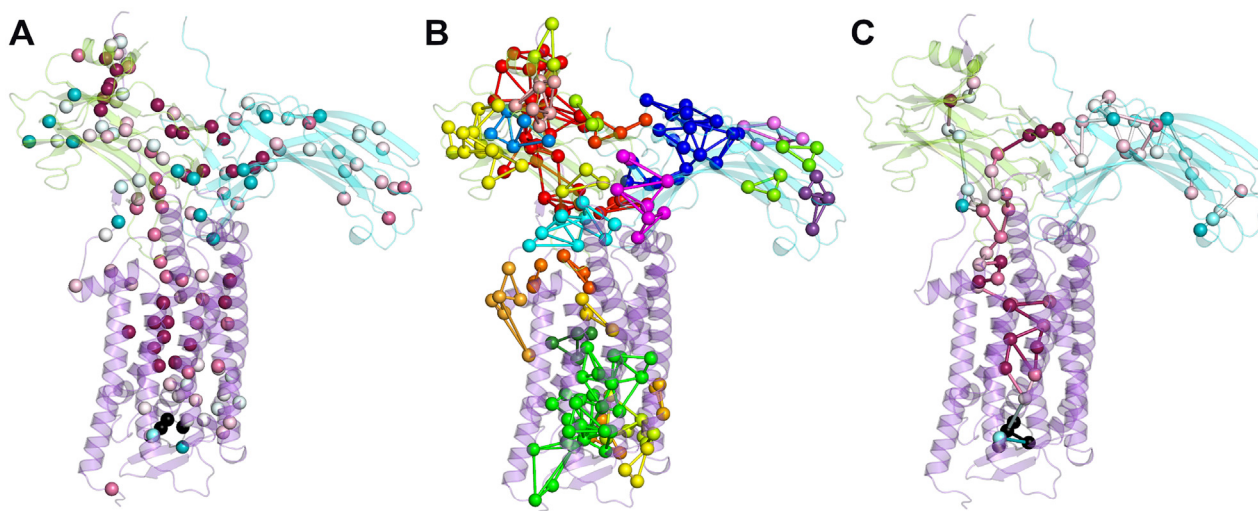
Fig. 9. Hub and community distributions and global metapath mapped on the ternary complex. A. The amino acids that act as stable hubs are shown colored according to the conservation grades inferred by the ConSurf web server (http://consurf.tau.ac.il). Hubs are represented as spheres centered on the Cα-atoms. B. Stable node communities are shown, colored according to the number of community nodes, the largest community being red. C. The global metapath is shown, colored according to the conservation grades inferred by the ConSurf web server (http://consurf.tau.ac.il). Black nodes and links in panels A and C belong to AVP. The cartoons of V2R and AVP are violet and black, respectively. The cartoons of ND and CD of β-arr1 are lemon-green and aquamarine, respectively. All pictures concern the MD trajectory frame closest to the average structure. (For interpretation of the references to color in this figure legend, the reader is referred to the web version of this article.)

differences between two different proteins or functional forms of the same protein as hyperlinked regions enriched in hubs are expected to hold higher structural stability and lower flexibility.

The allosteric communication in the ternary complex involving receptor, peptide agonist, and β-arr1 was investigated by computation of all possible shortest communication pathways according to a methodology already described [24,26,34,61]. A coarse view of the global communication propensity was inferred through the global metapath, i.e. a coarse path made of the most recurrent nodes and links in the path pool (see Methods). According to their definition, metapaths catch the
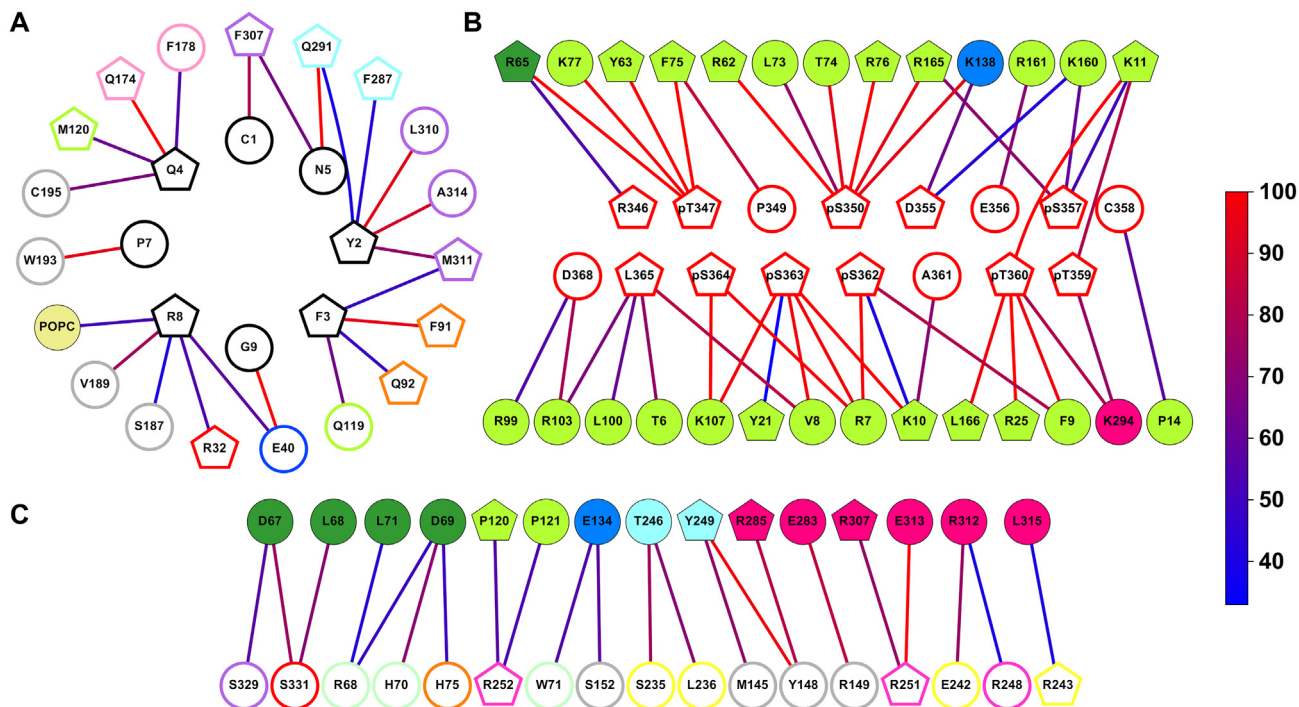
Fig. 10. Stable links at AVP-V2R and V2R-arrestin interfaces. The 2D-structure graphs of the AVP-V2R (A) as well as the V2R-arrestin primary (B) and secondary (C) interfaces are shown. Nodes are represented as circles whereas hubs are represented as pentagons. The V2R and AVP nodes are unfilled, whereas arrestin nodes are filled. Hubs and nodes are colored according to the protein portions they belong to. In detail, AVP is black and the V2R H1, H2, H3, H4, H5, H6, H7, and H8 are, respectively, blue, orange, lemon-green, pink, yellow, aquamarine violet, and red, whereas N-terminus/C-terminus, IL1/EL1, IL2/EL2, and IL3/EL3 are, respectively, red, slate, gray, and magenta. As for β-arr1, finger loop, middle loop, lariat loop, ND, and CD are, respectively, yellow, gray, dark-green, blue, hot-pink, and lemon-green, and aquamarine, respectively. Links are colored according to their frequency, as shown in the color bar on the right. (For interpretation of the references to color in this figure legend, the reader is referred to the web version of this article.)

most crucial information flow in the network.

As inferred from previous studies on other systems, hubs tend to correspond to highly conserved amino acid residues [26,28,29,31,35]. In the simulated ternary complex, V2R holds 58 stable hubs, of which 32 (55%) are conserved amino acids (i.e. holding ConSurf grades ≥7) almost all (84%) located in the cytosolic half of the receptor and including, among the others, the most conserved amino acids in H1 and H2 (i.e. N55(1.50) and D85(2.50)) as well as members of the FxxCWxPY and NPxxY motifs in H6 and H7, respectively (Fig. 9A, Table S2). Hubs crowd also in the AVP binding site but corresponding to less conserved amino acids (Figs. 9A and 10A). The AVP peptide holds as well four persistent hubs, i.e. Y2, F3, Q4, and R8 (Figs. 9A and 10A).

The receptor portions more frequently linked to AVP include EL2 and all helices but H5 (Fig. 10A). Remarkably, all phosphorylated amino acids in V2RCt behave as stable hubs (Figs. 9A and 10B). The majority (72%) of the 32 highly conserved V2R amino acids behaving as hubs also hold force constant values ≥ the average, whereas for the 26 non-conserved amino acid-hubs such percentage lowers to 38%. Stable hubs in β-arr1 are 74, of which 41 belong to ND and 33 to CD. 63% (26 out of 41) of the ND hubs are conserved amino acids, whereas such ratio lowers to 48% for CD hubs (Fig. 9A). Almost 46% of conserved amino acids-hubs in ND participate in the interface with V2R, with prominence to V2RCt. For β-arr1, the relation between amino acid-hub conservation and force constant is weaker compared to V2R. Collectively, 61% of ND hubs and 57% of CD hubs hold force constant values ≥ the average.

PSN analysis remarked the existence of two distinct receptor-arrestin interfaces: the primary and secondary interfaces. V2R participates in the primary interface with H8 and the C-tail. The β-arr1 portions participating in the primary interface comprise: the strands β1, β2, β5, β6, and β10 as well as the loops β1–β2, β2–β3, β6–β7, β9–β10, finger, middle, and lariat (Fig. 10B). The interface is made of 43 links, of which the majority (i.e. 40) holds a frequency ≥ 50% in the trajectory frames. Those links involve 16 nodes (including 11 hubs) from V2RCt, 27 nodes (including 10 hubs) from the ND, and 1 hub from the CD (Fig. 10B). The V2R portions contributing to the secondary interface comprise the cytosolic ends of H2, H5, and H8 as well as IL1, IL2, and IL3, whereas the β-arr1 portions include: the C-loop and the following strand as well as the loops β7–β8, finger, middle, and lariat (i.e. gate and back loops) (Fig. 10C). The interface is made of 22 links, of which the majority (i.e. 18) holds a frequency ≥50% in the trajectory frames. Those links involve 17 nodes (including 3 hubs) from V2R and 15 nodes (including 3 hubs) from β-arr1 (Fig. 10C).

Collectively, the majority of hubs both in V2R and in β-arr1 are highly conserved amino acids that crowd in the cytosolic half of V2R and in ND of β-arr1 at the interface with V2RCt. Remarkably, V2R contributes to the primary interface with one node less but a four-time higher number of hubs and a double number of links compared to the secondary interface. Moreover, β-arr1 contributes to the primary interface with 12 nodes more compared to the secondary interface. This is suggestive of higher stability of the former interface compared to the latter. This conclusion is also reflected by the interaction strength at the interface that is higher for the primary interface compared to the other. Indeed, for the primary interface, total and average strengths (expressed as percentages, see the Theory/Calculation section) of stable links are 424.38 and 9.87, respectively, whereas, for the secondary interface, total and average strengths of such links are 143.32 and 6.51, respectively. Inversely, the two proteins bury a smaller surface at the primary interface than at the secondary interface (Fig. S8).

Consistent with hub distribution, the largest community of nodes (colored red in Fig. 9B) involves the primary interface between β-arr1 and V2RCt, whereas the second community in size (colored green in Fig. 9B) involves the AVP binding site and part of the cytosolic half of the receptor (Table S3). The secondary receptor-arrestin interface participates essentially in two small communities, which strengthens the hypothesis that such interface is less stable and more dynamic than the

primary one.

The analysis of shortest communication pathways highlights the existence of an allosteric communication between AVP and β-arr1 (Table S4 and Fig. 9C). The information transfer is likely mediated by the interaction between the functionally relevant Y2 of AVP and F287(6.51), which constitutes one of the two links between the peptide agonist and the receptor in the global metapath. The latter depicts a communication that starts from AVP, involves highly conserved amino acids in H6, H7, H3, H2, H1, and H8, passes on β-arr1 through links between H8 and the finger loop, and divides in two branches. One branch involves the interface between V2RCt and the ND via the strand β6, whereas the other passes through β5, β6, and β8 in ND, extending to CD (Fig. 9C). Remarkably, the first two metapath links in CD following those in ND locate on the back loop and on the arrestin C-tail. Collectively, the ND of β-arr1 is primarily involved in the allosteric communication with V2R. The majority of the 61 links in the metapath, involves at least one conserved amino acid, i.e. 45 (74%), and at least one hub, i.e. 48 (79%). Eight metapath-links, which are located close to or at the secondary receptor-arrestin interface, if eliminated, reduce by at least 55% the number of links participating in the original metapath.

Collectively, the following highlights could be inferred from the PSN analysis. 1. Hubs tend to correspond to highly conserved amino acid residues, which locate on the cytosolic half of V2R and on the ND of β-arr1. 2. For both receptor and arrestin, stable hubs correspond to relatively high mechanical rigidity points. 3. All phosphorylated amino acids in V2RCt behave as stable hubs. 4. Two dynamically distinct interfaces characterize the V2R-arrestin complex, the one between V2RCt and β-arr1-ND being characterized by stronger and more stable inter-protein contacts than the other. 5. Similar to the primary receptor-arrestin interface, involved in the largest node community, the AVP binding site is crowded of hubs and, consistently, is involved in the second largest community. 6. The two largest node communities, at two distal poles of the ternary complex, are in allosteric communication between each other. 7. An allosteric communication mediated by highly conserved amino acids of V2R, indeed, exists between AVP and the ND of β-arr1.

4. Discussion

GPCRs are critically regulated by arrestins, which not only desensitize G-protein signaling but also initiate a G protein-independent wave of signaling [70–72]. Recent high-resolution structural data on a number of GPCRs in complex with functionally different ligands as well as with G proteins provided insights into the mechanism of GPCR activation and their action as GEFs [73]. However, complementary information has been lacking on the recruitment of β-arrestins to activated GPCRs, primarily owing to challenges in obtaining stable receptor-β-arrestin complexes for structural studies [13]. When we started the study, information at the atomic detail concerned the crystal structure of β-arr1 in complex with fully phosphorylated V2RCt [12] and visual arrestin in complex with phosphorylated rod opsin [15,17,19]. Such information was indeed exploited to build a structural model of the ternary complex comprising fully phosphorylated V2R, the agonist AVP, and β-arr1, and to infer dynamics and structural communication properties. The β-arr1 state employed in this study [12], indeed, would represent the one able to recognize an active state of the receptor.

Our molecular simulations retained the original contacts between the cationic amino acid residues in sites A-D of β-arr1 and the eight phosphorylated amino acid residues of V2RCt, which is linked to disruption of the polar core and displacement of the highly dynamic C-tail of β-arr1. In this respect, fully phosphorylated V2RCt forms a stable anti-parallel β-sheet with the finger loop, which is in turn constrained to dock in between H8 and IL1 of V2R, being unable to interact with H6, as found in the complexes between opsin and visual arrestin [15,17]. In spite of the differences between the two arrestins, the two

receptors, and the number of phosphorylated sites (eight vs two, respectively), the orientation of V2R and β-arr1 in the simulated complex is similar to that of opsin and visual arrestin, while it differs substantially from that predicted for chimeric β2-AR/V2RCt in complex with β-arr1 [13]. The latter is indeed incompatible with the interactions between V2RCt and D site of β-arr1, present in the crystal structure. It has been speculated that such incongruence with the crystal structure is due to the fact that the V2RCt in the chimeric receptor is mobile and repositions itself markedly upon β-arr1 interaction with the receptor core [13]. Our results, however, suggest that high mobility of V2RCt is incompatible with full phosphorylation and with all phosphorylated amino acids engaged in salt bridges with cationic amino acids of arrestin. In our system, the RTPPSLGPQDE**SCTTASS**SLAKD C-terminal sequence of V2R, where the bold underlined letters indicate the **PxxPxxP** phosphorylation code (long code) predicted for high-affinity arrestin binding [17], all the eight serines and threonines are phosphorylated. In contrast, in opsin complexed with visual arrestin, only T336 and S338 (recognizing, respectively, the A and B cationic sites of visual arrestin) are phosphorylated, thus contributing to the different conformation and orientation of the finger loop, which holds a two-turn helix, and to the higher mobility of the opsin C-tail, which reflect on the secondary receptor-arrestin interface. Full phosphorylation structurally and dynamically integrates the V2RCt into the β-arr1 ND and may not allow the finger loop to adopt an α-helix conformation. Incidentally, the buried surface area of the V2R-β-arr1 complex is greater than that of opsin-visual arrestin complex, i.e. respectively 3390 ± 138 Å^2 (as a median value) and 2420 Å^2 (measured on the crystallographic complex [17]). This may be due, at least in part, to the more extended interface 1 in the former complex compared to the latter.

Full phosphorylation of V2RCt also exacerbates the differences in strength and flexibility of the primary and secondary interfaces, which is consistent with the postulated sequential steps of receptor-arrestin recognition, the first step consisting in formation of the primary interface essential for high affinity binding and for the trigger of the conformational changes necessary to form the secondary interface with the receptor core [3]. The latter is weaker than the former and is made of several small β-arr1 patches including the finger, middle, gate, and back loops (the latter two being parts of the lariat loop). Remarkably, the secondary interface involves, among others, contacts between V2R IL2 and the β-arr1 middle loop (e.g. $S152_{V2R}$-$E134_{β-arr1}$), the strand that follows the C-loop (e.g. $Y148_{V2R}$-$Y249_{β-arr1}$), and the gate loop (e.g. $R149_{V2R}$-$E283_{β-arr1}$). This is consistent with evidence that mutation of the residues distal to the DRY motif (at the end of H3) would affect β-arrestin recruitment for a number of GPCRs [74]. Contacts between V2R IL3 and arrestin back loop (e.g. $R251_{V2R}$-$E313_{β-arr1}$) may contribute as well to arrestin recognition/activation.

Collectively, consistent with the opsin-visual arrestin complex, the secondary interface in the V2R-β-arr1 complex is such that it precludes binding of the G protein, which would contribute to the mechanism of GPCR desensitization. This occurs even if the finger loop does not dock in between H3 and H6 as it does in the opsin-arrestin complex, due to the full phosphorylation of V2RCt.

The complex between the M2R/V2RCt chimera and β-arr1 released when this study was under review [21] shows that the finger loop is flipped and the β-strand following the loop is shorter and not involved in an antiparallel β-sheet with the V2RCt. The region 346–353 is completely disordered and the interaction between pT347 with both R65 and K77 (both in the cationic D site of β-arr1) and between pS350 and both K138 and R75 (in the A site) are unlikely to occur. This may be due to the fact that pT347 and pS350 are not phosphorylated, and/or that the chimeric V2RCt is quite mobile, and/or the cryo-EM complex represents a more advanced receptor-arresting recruitment stage than the one simulated here. It has been hypothesized that, in a multi-step binding process, the formation of the final complex would require the release of the N-terminus of the receptor phosphopeptide, flipping of the finger loop of β-arr1, and burial of the finger loop in the cytosolic

receptor cavity, which overlaps with the one recognized by the G protein [21].

Arrestin activation has been found associated with the inter-domain twist, possibly instrumental in exposing interaction surfaces to intracellular binding partners [11,12,15,17,18]. Indeed, inter-domain twist was over-emphasized in recent computational experiments on visual arrestin activation by rod opsin, in which that geometrical descriptor was used as a unique structural hallmark of presence or absence of arrestin activation [75]. Simulations on structural models from the crystal structure of the rod opsin-arrestin complex, removing either the receptor C-tail (leaving only the receptor core) or the receptor core (leaving only the receptor C-tail) showed that, in each case, the CD remained close to its active-state position, although not as consistently as when the entire receptor was present [75]. They found average inter-domain twist angles of $15.6 \pm 5.1°$ with only the receptor core bound, $17.0 \pm 5.1°$ with only the receptor C-tail bound, and $20.6 \pm 4.4°$ with both core and C-tail bound. On those bases they concluded that the receptor core and the receptor C-tail each individually stabilize the active conformation of arrestin, though binding of both together stabilizes it further [75]. Yet, a 20°/21° twist-angle value characterizes active arrestin states totally independent of the presence of receptor or bound only to the phosphorylated receptor C-tail [11,12,18]. The very recent crystal structures of β-arr1 in complex with M2R/V2RCt and NTSR1 displayed, respectively, 16.6° and 16.0° twist angles, thus remarking the structural plasticity of arrestins even in the same functional state. Herein, we found that the inter-domain twist angle correlates with the essential motion sub-space explored by the ternary complex, thus confirming its relevance in the context of arrestin dynamics. It tends to stay close to but lower than the initial value (21°). Functional mode analysis suggests that inter-domain twist, linked to the two arrestin domains behaving as dynamically independent from each other, is assisted by the receptor, which acts distinctly at the primary and secondary interfaces with β-arr1, as well as by the membrane that persistently interacts with the CD. While the motion of β-arr1 ND is correlated with that of the receptor, the same does not happen for the CD. The analysis of the overall fluctuations and of the essential dynamics revealed a coupling between the agonist binding site of V2R, in the presence of AVP, and the ND of β-arr1. Indeed, the two distal regions undergo large distance fluctuations and participate in the highest amplitude collective motions. The agonist binding site and the interface between V2RCt and ND participate in the two largest node communities. Allosteric communication pathways pass through those node communities and involve highly conserved amino acids in the cytosolic halves of the transmembrane helices and in H8. Links at the interface between H8 and finger loop are central in the establishment of such communication, which is likely favored by full phosphorylation of V2RCt. Remarkably, the agonist binding site communicates with the first amino acid of β-arr1 C-tail, which is highly mobile as an effect of arrestin activation.

The β-arr1 CD contains stable anchor points to the membrane, which is essential for the maximal coupling to the receptor and is critical for receptor desensitization and internalization [21].

The inferences from PSN analysis agree with the demonstrated relationship between amino acid mechanical rigidity and evolutionary conservation [76]. Indeed the hubs, which correspond to mechanical rigidity points, tend to be highly conserved amino acids.

Collectively, the present study investigated structure and dynamics of the ternary complex involving V2R, AVP, and β-arr1 in full phosphorylation conditions. The latter limit the dynamics of both V2RCt, which is profoundly integrated in β-arr1 ND, and the secondary receptor-arrestin interface. Full phosphorylation also favors the allosteric communication between agonist binding site and β-arr1 ND, through a dynamic coupling between the two regions. Mechanical rigidity points, often acting as hubs in the structure network and distributed along the main axis of the receptor helix bundle, contribute to establish a preferential communication pathway between agonist ligand and the ND of

arrestin. Such pathway involves the primary interface more extensively than the second. Changes in the phosphorylation extent of the C-tail or a shift of phosphorylation from the C-tail to other regions of the receptor may induce changes in the architecture of the receptor-arrestin complex and the consequent way, in which signal transfer between agonist ligand and desensitizing protein occurs.

We cannot exclude that formation of a fully productive V2R-arrestin complex would require a partially phosphorylated V2RCt especially in its N-terminal extremity, which would allow the finger loop to adopt different conformations/orientations and to reach the receptor cavity between H3 and H6, as in the complex between opsin and visual arrestin and the complexes between M2R/V2RCt or NTSR1 and β-arr1. If instead, full phosphorylation is associated with a fully active ternary complex, we should conclude that the last stages in the process of arrestin recruitment would require the release of the interactions involving at least two (the most N-terminal) of the eight phosphorylated amino acids of V2RCt. In that respect, the effects of phosphorylation deserve future investigation.

All together, the results of the present investigation and the advances in structure determinations strengthen the concept that a network of diversified low-affinity interactions involving both receptor and phospholipids provide only two β-arrestin isoforms with the necessary plasticity to recognize hundreds of differently phosphorylated GPCRs.

Supplementary data to this article can be found online at https://doi.org/10.1016/j.bbamem.2020.183355.

Author contribution

LB performed MD simulations; AF performed MD analyses and contributed to manuscript writing; FF conceived the study, modeled the ternary complex, analyzed the data and wrote the manuscript.

Declaration of competing interest

The authors declare that they have no known competing financial interests or personal relationships that could have appeared to influence the work reported in this paper.

Acknowledgements

References

[1] K.L. Pierce, R.T. Premont, R.J. Lefkowitz, Seven-transmembrane receptors, Nat. Rev. Mol. Cell Biol. 3 (2002) 639–650.

[2] J.R. Hepler, A.G. Gilman, G-proteins, Trends Biochem. Sci. 17 (1992) 383–387.

[3] V.V. Gurevich, E.V. Gurevich, The molecular acrobatics of arrestin activation, Trends Pharmacol. Sci. 25 (2004) 105–111.

[4] C.E. Alvarez, On the origins of arrestin and rhodopsin, BMC Evol. Biol. 8 (2008) 222.

[5] L.M. Luttrell, S.S. Ferguson, Y. Daaka, W.E. Miller, S. Maudsley, G.J. Della Rocca, F. Lin, H. Kawakatsu, K. Owada, D.K. Luttrell, M.G. Caron, R.J. Lefkowitz, Beta-arrestin-dependent formation of beta2 adrenergic receptor-Src protein kinase complexes, Science 283 (1999) 655–661.

[6] P.H. McDonald, C.W. Chow, W.E. Miller, S.A. Laporte, M.E. Field, F.T. Lin, R.J. Davis, R.J. Lefkowitz, Beta-arrestin 2: a receptor-regulated MAPK scaffold for the activation of JNK3, Science 290 (2000) 1574–1577.

[7] J. Granzin, U. Wilden, H.W. Choe, J. Labahn, B. Krafft, G. Buldt, X-ray crystal structure of arrestin from bovine rod outer segments, Nature 391 (1998) 918–921.

[8] J.A. Hirsch, C. Schubert, V.V. Gurevich, P.B. Sigler, The 2.8 A crystal structure of visual arrestin: a model for arrestin's regulation, Cell 97 (1999) 257–269.

[9] M. Han, V.V. Gurevich, S.A. Vishnivetskiy, P.B. Sigler, C. Schubert, Crystal structure of beta-arrestin at 1.9 angstrom: possible mechanism of receptor binding and membrane translocation, Structure 9 (2001) 869–880.

[10] X. Zhan, L.E. Gimenez, V.V. Gurevich, B.W. Spiller, Crystal structure of arrestin-3 reveals the basis of the difference in receptor binding between two non-visual

[11] Y.J. Kim, K.P. Hofmann, O.P. Ernst, P. Scheerer, H.W. Choe, M.E. Sommer, Crystal structure of pre-activated arrestin p44, Nature 497 (2013) 142–146.

[12] A.K. Shukla, A. Manglik, A.C. Kruse, K.H. Xiao, R.I. Reis, W.C. Tseng, D.P. Staus, D. Hilger, S. Uysal, L.Y. Huang, M. Paduch, P. Tripathi-Shukla, A. Koide, S. Koide, W.I. Weis, A.A. Kossiakoff, B.K. Kobilka, R.J. Lefkowitz, Structure of active beta-arrestin-1 bound to a G-protein-coupled receptor phosphopeptide, Nature 497 (2013) 137–141.

[13] A.K. Shukla, G.H. Westfield, K. Xiao, R.I. Reis, L.Y. Huang, P. Tripathi-Shukla, J. Qian, S. Li, A. Blanc, A.N. Oleskie, A.M. Dosey, M. Su, C.R. Liang, L.L. Gu, J.M. Shan, X. Chen, R. Hanna, M. Choi, X.J. Yao, B.U. Klink, A.W. Kahsai, S.S. Sidhu, S. Koide, P.A. Penczek, A.A. Kossiakoff, V.L. Woods Jr, B.K. Kobilka, G. Skiniotis, R.J. Lefkowitz, Visualization of arrestin recruitment by a G-protein-coupled receptor, Nature 512 (2014) 218–222.

[14] M. Szczepek, F. Beyriere, K.P. Hofmann, M. Elgeti, R. Kazmin, A. Rose, F.J. Bartl, D. von Stetten, M. Heck, M.E. Sommer, P.W. Hildebrand, P. Scheerer, Crystal structure of a common GPCR-binding interface for G protein and arrestin, Nat. Commun. 5 (2014) 4801.

[15] Y. Kang, X.E. Zhou, X. Gao, Y. He, W. Liu, A. Ishchenko, A. Barty, T.A. White, O. Yefanov, G.W. Han, Q. Xu, P.W. de Waal, J. Ke, M.H. Tan, C. Zhang, A. Moeller, G.M. West, B.D. Pascal, N. Van Eps, L.N. Caro, S.A. Vishnivetskiy, R.J. Lee, K.M. Suino-Powell, X. Gu, K. Pal, J. Ma, X. Zhi, S. Boutet, G.J. Williams, M. Messerschmidt, C. Gati, N.A. Zatsepin, D. Wang, D. James, S. Basu, S. Roy-Chowdhury, C.E. Conrad, J. Coe, H. Liu, S. Lisova, C. Kupitz, I. Grotjohann, R. Fromme, Y. Jiang, M. Tan, H. Yang, J. Li, M. Wang, Z. Zheng, D. Li, N. Howe, Y. Zhao, J. Standfuss, K. Diederichs, Y. Dong, C.S. Potter, B. Carragher, M. Caffrey, H. Jiang, H.N. Chapman, J.C. Spence, P. Fromme, U. Weierstall, O.P. Ernst, V. Katritch, V.V. Gurevich, P.R. Griffin, W.L. Hubbell, R.C. Stevens, V. Cherezov, K. Melcher, H.E. Xu, Crystal structure of rhodopsin bound to arrestin by femtosecond X-ray laser, Nature 523 (2015) 561–567.

[16] P. Scheerer, M.E. Sommer, Structural mechanism of arrestin activation, Curr. Opin. Struct. Biol. 45 (2017) 160–169.

[17] X.E. Zhou, Y.Z. He, P.W. de Waal, X. Gao, Y.Y. Kang, N. Van Eps, Y.T. Yin, K. Pal, D. Goswami, T.A. White, A. Barty, N.R. Latorraca, H.N. Chapman, W.L. Hubbell, R.O. Dror, R.C. Stevens, V. Cherezov, V.V. Gurevich, P.R. Griffin, O.P. Ernst, K. Melcher, H.E. Xu, Identification of phosphorylation codes for arrestin recruitment by G protein-coupled receptors, Cell 170 (2017) 457–469.

[18] Q.Y. Chen, N.A. Perry, S.A. Vishnivetskiy, S. Berndt, N.C. Gilbert, Y. Zhuo, P.K. Singh, J. Tholen, M.D. Ohi, E.V. Gurevich, C.A. Brautigam, C.S. Klug, V.V. Gurevich, T.M. Iverson, Structural basis of arrestin-3 activation and signaling, Nat. Commun. 8 (2017) 1427.

[19] X.E. Zhou, X. Gao, A. Barty, Y.Y. Kang, Y.Z. He, W. Liu, A. Ishchenko, T.A. White, O. Yefanov, G.W. Han, Q.P. Xu, P.W. de Waal, K.M. Suino-Powell, S. Boutet, G.J. Williams, M.T. Wang, D.F. Li, M. Caffrey, H.N. Chapman, J.C.H. Spence, P. Fromme, U. Weierstall, R.C. Stevens, V. Cherezov, K. Melcher, H.E. Xu, X-ray laser diffraction for structure determination of the rhodopsin-arrestin complex, Sci. Data 3 (2016) 160021.

[20] R.H. Oakley, S.A. Laporte, J.A. Holt, M.G. Caron, L.S. Barak, Differential affinities of visual arrestin, beta arrestin1, and beta arrestin2 for G protein-coupled receptors delineate two major classes of receptors, J. Biol. Chem. 275 (2000) 17201–17210.

[21] D.P. Staus, H. Hu, M.J. Robertson, A.L.W. Kleinhenz, L.M. Wingler, W.D. Capel, N.R. Latorraca, R.J. Lefkowitz, G. Skiniotis, Structure of the M2 muscarinic receptor-beta-arrestin complex in a lipid nanodisc, Nature 579 (2020) 297–302.

[22] W. Huang, M. Masureel, Q. Qu, J. Janetzko, A. Inoue, H.E. Kato, M.J. Robertson, K.C. Nguyen, J.S. Glenn, G. Skiniotis, B.K. Kobilka, Structure of the neurotensin receptor 1 in complex with beta-arrestin 1, Nature 579 (2020) 303–308.

[23] M. Seeber, A. Felline, F. Raimondi, S. Muff, R. Friedman, F. Rao, A. Caflisch, F. Fanelli, Wordom: a user-friendly program for the analysis of molecular structures, trajectories, and free energy surfaces, J. Comput. Chem. 32 (2011) 1183–1194.

[24] M. Seeber, A. Felline, F. Raimondi, S. Mariani, F. Fanelli, WebPSN: a web server for high-throughput investigation of structural communication in biomacromolecules, Bioinformatics 31 (2015) 779–781.

[25] S. Mariani, D. Dell'Orco, A. Felline, F. Raimondi, F. Fanelli, Network and atomistic simulations unveil the structural determinants of mutations linked to retinal diseases, PLoS Comput. Biol. 9 (2013) e1003207.

[26] F. Raimondi, A. Felline, G. Portella, M. Orozco, F. Fanelli, Light on the structural communication in Ras GTPases, J. Biomol. Struct. Dyn. 31 (2013) 142–157.

[27] A. Felline, S. Mariani, F. Raimondi, L. Bellucci, F. Fanelli, Structural determinants of constitutive activation of Gα proteins: transducin as a paradigm, J. Chem. Theory Comput. 13 (2017) 886–899.

[28] F. Fanelli, M. Seeber, Structural insights into retinitis pigmentosa from unfolding simulations of rhodopsin mutants, FASEB J. 24 (2010) 3196–3209.

[29] K. Angelova, A. Felline, M. Lee, M. Patel, D. Puett, F. Fanelli, Conserved amino acids participate in the structure networks deputed to intramolecular communication in the lutropin receptor, Cell. Mol. Life Sci. 68 (2011) 1227–1239.

[30] F. Fanelli, A. Felline, Uncovering GPCR and G protein function by protein structure network analysis, Comput. Tools Chem. Biol. (2017) 198–220.

[31] P. Behnen, A. Felline, A. Comitato, M.T. Di Salvo, F. Raimondi, S. Gulati, S. Kahremany, K. Palczewski, V. Marigo, F. Fanelli, A small chaperone improves folding and routing of rhodopsin mutants linked to inherited blindness, iScience 4 (2018) 1–19.

[32] F. Raimondi, A. Felline, F. Fanelli, Catching functional modes and structural communication in Dbl family rho guanine nucleotide exchange factors, J. Chem. Inf. Model. 55 (2015) 1878–1893.

[33] A. Felline, L. Belmonte, F. Raimondi, L. Bellucci, F. Fanelli, Interconnecting flexibility, structural communication, and function in RhoGEF Oncoproteins, J. Chem.

Inf. Model. 59 (2019) 4300–4313.

[34] F. Raimondi, A. Felline, M. Seeber, S. Mariani, F. Fanelli, A mixed protein structure network and elastic network model approach to predict the structural communication in biomolecular systems: the PDZ2 domain from tyrosine phosphatase 1E as a case study, J. Chem. Theory Comput. 9 (2013) 2504–2518.

[35] A. Felline, M. Ghitti, G. Musco, F. Fanelli, Dissecting intrinsic and ligand-induced structural communication in the beta3 headpiece of integrins, Biochim. Biophys. Acta 1861 (2017) 2367–2381.

[36] F. Fanelli, P.G. De Benedetti, Update 1 of: computational modeling approaches to structure-function analysis of G protein-coupled receptors, Chem. Rev. 111 (2011) PR438–535.

[37] A. Sali, T.L. Blundell, Comparative protein modelling by satisfaction of spatial restraints, J. Mol. Biol. 234 (1993) 779–815.

[38] W. Huang, A. Manglik, A.J. Venkatakrishnan, T. Laeremans, E.N. Feinberg, A.L. Sanborn, H.E. Kato, K.E. Livingston, T.S. Thorsen, R.C. Kling, S. Granier, P. Gmeiner, S.M. Husbands, J.R. Traynor, W.I. Weis, J. Steyaert, R.O. Dror, B.K. Kobilka, Structural insights into micro-opioid receptor activation, Nature 524 (2015) 315–321.

[39] F. Fanelli, Modeling the structural communication in supramolecular complexes involving GPCRs, Methods Mol. Biol. 914 (2012) 319–336.

[40] C. Barberis, B. Mouillac, T. Durroux, Structural bases of vasopressin/oxytocin receptor function, J. Endocrinol. 156 (1998) 223–229.

[41] B. Mouillac, B. Chini, M.N. Balestre, J. Elands, S. Trumppkallmeyer, J. Hoflack, M. Hibert, S. Jard, C. Barberis, The binding-site of neuropeptide vasopressin V1a receptor - evidence for a major localization within transmembrane regions, J. Biol. Chem. 270 (1995) 25771–25777.

[42] J.A. Ballesteros, H. Weinstein, Integrated methods for the construction of three-dimensional models and computational probing of structure-function relations in G protein-coupled receptors, Methods Neurosci. 25 (1995) 366–428.

[43] K. Fahmy, F. Jager, M. Beck, T.A. Zvyaga, T.P. Sakmar, F. Siebert, Protonation states of membrane-embedded carboxylic acid groups in rhodopsin and metarhodopsin II: a Fourier-transform infrared spectroscopy study of site-directed mutants, Proc. Natl. Acad. Sci. U. S. A. 90 (1993) 10206–10210.

[44] K.P. Hofmann, P. Scheerer, P.W. Hildebrand, H.W. Choe, J.H. Park, M. Heck, O.P. Ernst, A G protein-coupled receptor at work: the rhodopsin model, Trends Biochem. Sci. 34 (2009) 540–552.

[45] J.C. Phillips, R. Braun, W. Wang, J. Gumbart, E. Tajkhorshid, E. Villa, C. Chipot, R.D. Skeel, L. Kale, K. Schulten, Scalable molecular dynamics with NAMD, J. Comput. Chem. 26 (2005) 1781–1802.

[46] U. Essmann, L. Perera, M.L. Berkowitz, T. Darden, H. Lee, L.G. Pedersen, A smooth particle mesh Ewald method, J. Chem. Phys. 103 (1995) 8577–8593.

[47] J.P. Ryckaert, G. Ciccotti, H.J.C. Berendsen, Numerical-integration of Cartesian equations of motion of a system with constraints - molecular-dynamics of N-alkanes, J. Comput. Phys. 23 (1977) 327–341.

[48] M. Tuckerman, B.J. Berne, G.J. Martyna, Reversible multiple time scale molecular-dynamics, J. Chem. Phys. 97 (1992) 1990–2001.

[49] W.L. Jorgensen, J. Chandrasekhar, J.D. Madura, R.W. Impey, M.L. Klein, Comparison of simple potential functions for simulating liquid water, J. Chem. Phys. 79 (1983) 926–935.

[50] W. Humphrey, A. Dalke, K. Schulten, VMD: visual molecular dynamics, J. Mol. Graph. Mod. 14 (1996) 33–38.

[51] I. Navizet, F. Cailliez, R. Lavery, Probing protein mechanics: residue-level properties and their use in defining domains, Biophys. J. 87 (2004) 1426–1435.

[52] R. Lavery, S. Sacquin-Mora, Protein mechanics: a route from structure to function, J. Biosci. 32 (2007) 891–898.

[53] S. Sacquin-Mora, E. Laforet, R. Lavery, Locating the active sites of enzymes using mechanical properties, Proteins Struct. Funct. Bioinforma. 67 (2007) 350–359.

[54] M. Munz, J. Hein, P.C. Biggin, The role of flexibility and conformational selection in the binding promiscuity of PDZ domains, PLoS Comput. Biol. 8 (2012) e1002749.

[55] A. Amadei, A.B. Linssen, H.J. Berendsen, Essential dynamics of proteins, Proteins 17 (1993) 412–425.

[56] J.S. Hub, B.L. de Groot, Detection of functional modes in protein dynamics, PLoS Comput. Biol. 5 (2009) e1000480.

[57] S. Vishveshwara, K.V. Brinda, N. Kannan, Protein structure: insights from graph theory, J. Theor. Comput. Chem. 1 (2002) 187–211.

[58] S. Vishveshwara, A. Ghosh, P. Hansia, Intra and inter-molecular communications through protein structure network, Curr. Protein Pept. Sci. 10 (2009) 146–160.

[59] K.V. Brinda, S. Vishveshwara, A network representation of protein structures: implications for protein stability, Biophys. J. 89 (2005) 4159–4170.

[60] N. Kannan, S. Vishveshwara, Identification of side-chain clusters in protein structures by a graph spectral method, J. Mol. Biol. 292 (1999) 441–464.

[61] F. Fanelli, A. Felline, F. Raimondi, Network analysis to uncover the structural communication in GPCRs, Methods Cell Biol. 117 (2013) 43–61.

[62] E.W. Dijkstra, A note on two problems in connexion with graphs, Numer. Math. 1 (1959) 269–271.

[63] O.F. Lange, H. Grubmuller, Generalized correlation for biomolecular dynamics, Proteins 62 (2006) 1053–1061.

[64] H. Ashkenazy, S. Abadi, E. Martz, O. Chay, I. Mayrose, T. Pupko, N. Ben-Tal, ConSurf 2016: an improved methodology to estimate and visualize evolutionary conservation in macromolecules, Nucleic Acids Res. 44 (2016) W344–W350.

[65] S.M. Hanson, D.J. Francis, S.A. Vishnivetskiy, E.A. Kolobova, W.L. Hubbell, C.S. Klug, V.V. Gurevich, Differential interaction of spin-labeled arrestin with inactive and active phosphorhodopsin, Proc. Natl. Acad. Sci. U. S. A. 103 (2006) 4900–4905.

[66] S.A. Vishnivetskiy, C. Schubert, G.C. Climaco, Y.V. Gurevich, M.G. Velez, V.V. Gurevich, An additional phosphate-binding element in arrestin molecule - implications for the mechanism of arrestin activation, J. Biol. Chem. 275 (2000) 41049–41057.

[67] O.B. Goodman, J.G. Krupnick, F. Santini, V.V. Gurevich, R.B. Penn, A.W. Gagnon, J.H. Keen, J.L. Benovic, Beta-arrestin acts as a clathrin adaptor in endocytosis of the beta(2)-adrenergic receptor, Nature 383 (1996) 447–450.

[68] S.K. Vishnivetskiy, C.L. Paz, C. Schubert, J.A. Hirsch, P.B. Sigler, V.V. Gurevich, How does arrestin respond to the phosphorylated state of rhodopsin? J. Biol. Chem. 274 (1999) 11451–11454.

[69] C.C. Lally, B. Bauer, J. Selent, M.E. Sommer, C-edge loops of arrestin function as a membrane anchor, Nat. Commun. 8 (2017) 14258.

[70] R.J. Lefkowitz, S.K. Shenoy, Transduction of receptor signals by beta-arrestins, Science 308 (2005) 512–517.

[71] K.L. Pierce, R.J. Lefkowitz, Classical and new roles of beta-arrestins in the regulation of G-protein-coupled receptors, Nat. Rev. Neurosci. 2 (2001) 727–733.

[72] A.K. Shukla, K. Xiao, R.J. Lefkowitz, Emerging paradigms of beta-arrestin-dependent seven transmembrane receptor signaling, Trends Biochem. Sci. 36 (2011) 457–469.

[73] D. Hilger, M. Masureel, B.K. Kobilka, Structure and dynamics of GPCR signaling complexes, Nat. Struct. Mol. Biol. 25 (2018) 4–12.

[74] K.-M. Kim, M.G. Caron, Complementary roles of the DRY motif and C-terminus tail of GPCRS for G protein coupling and beta-arrestin interaction, Biochem. Biophys. Res. Commun. 366 (2008) 42–47.

[75] N.R. Latorraca, J.K. Wang, B. Bauer, R.J.L. Townshend, S.A. Hollingsworth, J.E. Olivieri, H.E. Xu, M.E. Sommer, R.O. Dror, Molecular mechanism of GPCR-mediated arrestin activation, Nature 557 (2018) 452–456.

[76] S. Sacquin-Mora, Fold and flexibility: what can proteins' mechanical properties tell us about their folding nucleus? J. R. Soc. Interface 12 (2015) 20150876.